PCCP

Photon catalysis of deuterium iodide photodissociation

Journal:	*Physical Chemistry Chemical Physics*
Manuscript ID	CP-ART-09-2018-006107.R1
Article Type:	Paper
Date Submitted by the Author:	n/a
Complete List of Authors:	Hilsabeck, Kallie; Stanford University, Chemistry Meiser, Jana; Stanford University, Chemistry Sneha, Mahima; Stanford University, Chemistry Naduvalath, Balakrishnan ; University of Nevada Las Vegas, Chemistry and Biochemistry Zare, Richard; Stanford University, Department of Chemistry

Article type: Full paper

Website www.rsc.org/pccp

Impact factor* 3.906

Journal expectations To be suitable for publication in *Physical Chemistry Chemical Physics* (*PCCP*) articles must include significant new innovation and/or insight into physical chemistry.

Article type: Full paper Original scientific work that has not been published previously. Full papers do not have a page limit and should be appropriate in length for scientific content.

Journal scope Visit the *PCCP* website for additional details of the journal scope and expectations.

PCCP is an international journal for the publication of cutting-edge original work in physical chemistry, chemical physics and biophysical chemistry. To be suitable for publication in *PCCP*, articles must include significant new innovation and/or insight into physical chemistry; this is the most important criterion that reviewers should judge against when evaluating submissions. Example topics within the journal's broad scope include:

- Spectroscopy
- Dynamics
- Kinetics
- Statistical mechanics
- Thermodynamics
- Electrochemistry
- Catalysis
- Surface science
- Quantum mechanics
- Theoretical research

Interdisciplinary research areas such as polymers and soft matter, materials, nanoscience, energy surfaces/interfaces, and biophysical chemistry are also welcomed if they demonstrate significant new innovation and/or insight into physical chemistry.

Reviewer responsibilities Visit the Reviewer responsibilities website for additional details of the reviewing policy and procedure for Royal of Society of Chemistry journals.

When preparing your report, please:

- Focus on the originality, importance, impact and reliability of the science. English language and grammatical errors do not need to be discussed in detail, except where it impedes scientific understanding.
- Use the journal scope and expectations to assess the manuscript's suitability for publication in *PCCP.*
- State clearly whether you think the article should be accepted or rejected and include details of how the science presented in the article corresponds to publication criteria.
- Inform the Editor if there is a conflict of interest, a significant part of the work you cannot review with confidence or if parts of the work have previously been published.

Thank you for evaluating this manuscript, your advice as a reviewer for *PCCP* is greatly appreciated.

Dr Katie Lim Executive Editor
Royal Society of Chemistry, UK

Professor Seong Keun Kim Editorial Board Chair
Seoul National University, South Korea

2016 Journal Citation Reports®, (Thomson Reuters, 2017)

Dear Editor,

We are grateful to the two reviewers for their comments, and all changes can be found in yellow highlight in a copy of the revised manuscript and the revised supporting information that we are submitting to you. What follows are the comments of the reviewers and our responses:

REVIEWER REPORT(S):
Referee: 1

Comments to the Author
This paper explores the effect of an intense non-resonant electric field on the molecular photodissociation dynamics of DI at excitation wavelengths between 210 nm and 280 nm. The intense electric field is provided by radiation from a nanosecond Nd:YAG laser at 1064 nm. Following photodissociation, the D atom photofragment is probed by (2+1) resonantly enhanced multiphoton ionization (REMPI), either in a conventional pump-probe arrangement or in a Doppler free configuration. The key experimental observable is the branching ratio between I and I*, which is derived from
integrating the associated peaks in the time-of-flight spectra of D+. The experiments are supported by model quantum wavepacket calculations performed using scaled excited potential energy curves.

The authors report changes in I/I* branching ratio at selected wavelengths between 210 nm and 280 nm on application of the non-resonant laser field. These changes are relatively small, but significant, and can only qualitatively be accounted for by the
wavepacket calculations.

This is a potentially interesting paper, but I have some reservations concerning the manuscript that I feel should be clarified before it would be suitable for publication.

i. It is unclear whether or not the scaled polarizabilities which were found necessary to qualitatively model the data are reasonable. Don't the original ab initio calculations provide the polarizabilities?

The original ab initio calculations do not provide polarizabilities (Reference 35). We have contacted authors of the paper, and they do not have data on the polarizabilities. Considering referee's comments, we carried out limited ab initio calculations without including spin-orbit couplings and obtained polarizabilities for the $^3\Pi$ and $^1\Pi$ states that are about a factor of 2-3 larger than the ground state, consistent with the values adopted for the shift2 potential. These calculations (see supplementary information) show that the excited state polarizabilities are much more anisotropic than the ground state. A more detailed calculation, including spin-orbit coupling, is beyond the scope of this work. A factor of 2-6 higher values for the polarizabilities of excited electronic states of LiH and NaH have been reported in the literature (Reference 33).

Changes to the manuscript
This explanation has been included on Page 7 of the manuscript, and additional details on the limited ab initio calculations are included in Page 7 of the Supplementary Information (Table S1).

ii. Is it reasonable that the effect of the intense field on the branching ratios varies from a suppression of I* at 216 nm to an enhancement at 230 nm? Given the very broad absorption features, the short dissociation timescales, and the relative insensitivityof the branching ratio and anisotropy parameters for the two channels to photolysis wavelength in the region in question, this dramatic change in behaviour over ~14 nm in the presence of a field seems surprising.

We agree that the enhancement at 230 nm is quite striking compared to the behavior observed at 216 nm; however, it is not necessarily unexpected. The decrease in the branching ratio at 216 nm can be explained in terms of a change in the relative probabilities for dissociation through two *adiabatic* product channels. This observation is qualitatively corroborated by a straightforward theoretical model that adequately describes how the cross-sections for excitation to and dissociation from a single electronic state (i.e., adiabatic transitions) are changed in the presence of a strong

field. Although previous studies report a predominately adiabatic picture of DI's dissociation dynamics, they also suggest a 7% contribution of nonadiabatic channels to the I^* product in the range of excitation wavelengths from 227-278 nm (References 15 and 29). We propose that, by shifting excited potential surfaces to different extents based upon their polarizabilities, the strong field influences the nonadiabatic dynamics more than the adiabatic dynamics and contributes to an increase in the I* product channel. It is likely that this nonadiabatic behavior, which cannot be fully described by our theoretical treatment, was experimentally observed at 230-nm excitation.

Previous experimental observations support this hypothesis. In the ultrafast study of photon-catalyzed IBr photodissociation, Albert Stolow and coworkers (Reference 1 in the manuscript) observed the greatest influence of the strong nonresonant field as an effect on the nonadiabatic dynamics. Experiments showed the maximum change in the branching ratio when the nonresonant pulse arrived as the wavepacket traversed a crossing. A 30% increase in Br* production resulted at this intersection, which is comparable to the increase we observed at 230 nm for DI. This experimental observation supports our claim that the influence of the electric field on the nonadiabatic dynamics *has the potential to* lead to such a large change in the observed branching ratio. Furthermore, it is clear from Stolow's study (Reference 1) that the induced change in the branching ratio rapidly (within hundreds of femtoseconds) decreased to zero when the nonresonant pulse was delayed beyond the time the molecule passed around the crossing. If we are accessing or inducing a crossing near 230-nm excitation, we expect a sensitive response to the excitation energy around the crossing: for excitation energies below or above the crossing, the molecule's hopping probability is not measurably affected, and nonadiabaticity does not play a large role in the dissociation dynamics.

Changes to the manuscript
This explanation has been included on page 13 of the manuscript as part of the discussion on the discrepancy between experiment and theory at 230 nm.

iii. The procedures for background subtraction are discussed in some detail in the supplementary information. It is clear that the background contributions to the signal are significant in some cases. It is perhaps a concern that the two data points which show an I* enhancement, at 230 nm and 265 nm, were obtained using a slightly different laser configuration than that employed at the other wavelengths studied. Did the authors try the same probe-delay scheme at 213 nm, 216 nm, 243 nm and 278 nm?

In response to this comment, it is important that we discuss the major differences between the two detection techniques, the factors that informed our choice of which technique to use, and the reasons why these choices do not contribute to a systematic bias in the result.

In our traditional pump-probe experiments, DI molecules are first dissociated by the pump laser and, after a short time delay of 3 ns, the resulting D-atom product is ionized using (2+1)-REMPI via the 2s – 1s transition at approximately 243 nm. The probe laser wavelength is scanned in 1-pm steps over the Doppler range and, at each wavelength, only a fraction of the product is ionized because of the distribution of speeds of the D-atoms relative to the direction of the probe laser's propagation. In the Doppler-free method, two counterpropagating UV lasers are overlapped spatially and temporally, and their wavelengths are chosen such that combined they achieve resonance with the (2+1)-REMPI line at 243 nm. Because both lasers are contributing to the probe step and are traveling in opposite directions toward the interaction region, D atoms are ionized regardless of their speed with respect to the laser propagation direction. This condition strongly increases the signal without impacting the amount of background in our experiments. Furthermore, as the Doppler-free technique relieves the requirement to perform a scan over the Doppler range, it removes inconsistencies which may arise because of power and degree of overlap fluctuations of the lasers throughout data collection. In these experiments, the overlap condition is vital to the measured effect. As also detailed in point v., this results in cleaner, more consistent experimental data and a significantly greater signal-to-background ratio.

Collectively, these differences make the Doppler-free configuration the more ideal one for our purposes. However, for 265 nm, the complementary UV wavelength required to fulfill the Doppler-free condition was 224 nm. The slow channel of 224 nm overlapped completely with the 265 nm fast channel, as now shown in Fig. S2 and Table S2 in the ESI. As this would have led to inaccuracies in our results, we used a conventional pump-probe method. At an excitation wavelength of 230 nm, the multiphoton background arising from the 257-nm UV laser overlap with the

IR overwhelmed the signal, producing very noisy data. To prevent that, we again chose to use the pump-probe technique. The 243-nm probe laser contributed to less multiphoton background and allowed us to offset the probe laser in time.

As pointed out by the reviewer, an increase in I* production is observed only for the wavelengths in which the pump-probe technique is used. We are not concerned by this coincidence for the following reasons:

1) Although the detection techniques were different for different excitation wavelengths, the background subtraction was performed in the same way. The only notable difference is the 3 ns delay used in the pump-probe experiments, which was introduced to reduce multiphoton UV probe laser + IR background while still collecting true signal. This delay affects the overall timing component to the background subtraction only marginally because of the durations of the pulses: 8-10 ns for the UV pulses, and 10-12 ns for the IR pulse. To prove this claim, the experiment was repeated at 0 ns delay at 230 nm to confirm that the increase to the slow channel was not the result of this experimental condition. Measured speed distributions and branching ratios were not influenced by a time delay of this magnitude, under either field-free or IR-field conditions.

2) We find no justification for a systematic bias towards an increase in the slow channel with a pump-probe scheme, outside of the time delay "missing" the faster channel ions which was discussed in point 1. This would only occur if a systematically lower amount of multiphoton background was subtracted at slower speeds relative to faster speeds for the pump-probe scans vs. the Doppler-free scans. There is no experimental cause for this to occur.

3) We also performed the field-free and IR field experiments at 243 nm using a one laser setup, which is like the pump-probe approach both in how the probing step is performed and the amount of background. In this setup, a single UV laser pulse at 243 nm photolyzes the DI and ionizes the product D atom. As was the case for the Doppler-free setup, we measured no change in the branching ratio with application of the IR-field (Fig. S4a and b). This supports our claim that the result is independent of the detection technique used to collect the data.

We did not perform the experiments at 213, 216, and 278 nm in the pump-probe laser configuration for comparison. For these wavelengths, the dissociation cross section for DI is less than or equal to the cross section at 243 nm (Reference 15). Therefore, 243 nm light contributed non-negligibly to background in 2 ways: 1) by directly dissociating the DI molecules and ionizing the product D atoms, and 2) by participating in UV + IR multiphoton processes. A lower signal-to-background ratio is expected in the presence of the strong field for the pump-probe technique relative to the Doppler-free technique, precluding the use of the former technique.

Changes to the manuscript
-A more complete description of the differences between the two techniques, as well as the choices that informed our decisions (Experimental details, pages 5,6).

-Figure S2 in the electronic supplementary information, which shows the overlapping peaks when the Doppler-free technique is used to collect data at 265 nm (page 5 of ESI).

-Modified Fig. S1 in the electronic supplementary information, to more clearly show that the 3 ns delay has a very small impact on the amount of overlap between the three lasers (page 4 of ESI).

-We elaborated on page 10 of the manuscript on the observation that both wavelengths employing the pump-probe technique yielded an increase in the slow channel. Additionally, data supporting that this is rather a coincidence than a systematic bias is presented in Fig. S4 a and b in the electronic supplementary information (Page 9), which shows both the Doppler-free and the pump-probe speed distributions for 243-nm dissociation.

iv. The time-of-flight profiles for the I* channel seem qualitatively different at 230 nm and 265 nm than the rather Gaussian looking profiles observed at the other wavelengths. Do the authors have an explanation for that? The 230 nm data seems to possess a shoulder at low velocities in the presence of a field, which is absent in the field free spectra. Again, why might that be the case?

To question 1: We attribute the more Gaussian peaks observed using the Doppler-free technique to the cleaner, more consistent nature of data collection relative to the traditional pump-probe approach. The Doppler-free technique is a

cleaner experiment in that D atoms in the focal volume are ionized regardless of their speed relative to the direction of laser propagation, increasing the signal without affecting the background. By taking away the need to perform a wavelength scan over the Doppler range, the Doppler-free condition affords us better control over power and overlap fluctuations of the lasers that occur throughout data collection which might contribute to variations in ionization yield and result in less Gaussian looking time-of-flight profiles.

To question 2: The 230-nm data were collected using the pump-probe method. Small amounts of dissociation by the probe laser at 243 nm led to the production of slow and fast channel D-atoms with velocities close to the slow and fast channel D-atoms from the desired excitation wavelength (Table S2). Although the signal corresponding to 243-nm dissociation is nearly entirely corrected for by the background subtraction method, a small shoulder remains on the leading edge of each 230-nm peak which is consistent with 243-nm dissociation. As the reviewer pointed out, these shoulders are more prevalent in the IR-field speed distributions than the field-free distributions. This could be the result of a higher ratio of pump laser power to probe laser power for the field-free experiments. However, it is also evident from Fig. 2c that the error bars in this speed region of the field-free distribution nearly extend to meet the error bars in the IR-field distributions. We conclude that, although they are significantly different to one standard deviation, the background from 243-nm dissociation exists under both field-free and IR-field conditions. This shoulder is not included in the area that is integrated for the branching ratio calculations. However, inclusion of the shoulder for both the slow and fast channel peaks does not cause the branching ratio to fall outside of the currently reported uncertainty also because the branching ratio at 243 nm is approximately equal to 1 for both the field-free and IR-field cases.

Changes to the manuscript
Question 1 has been addressed on page 6 of the manuscript, and a clarifying statement concerning question 2 was added on page 10.

v. The benefits of using the Doppler-free REMPI method are unclear, at least from consideration of the time-of-flight data presented in the paper.

In the traditional pump-probe scheme, the probe laser is scanned incrementally over the Doppler range and, at each wavelength, only a fraction of the product is ionized. In the Doppler-free method, D atoms are ionized regardless of their speed in the direction of laser propagation, thereby strongly increasing the signal without affecting the background. This aspect of the Doppler-free technique made it very advantageous because it allowed for a better signal-to-background ratio. Furthermore, the Doppler-free technique takes away inconsistencies which may arise because of power and overlap fluctuations of the lasers during a Doppler scan. For these reasons, the Doppler-free method was preferable for all wavelengths. However, at 265 nm, the complementary UV wavelength required to fulfill the Doppler-free condition was 224 nm. The slow channel of 224 nm completely overlapped with the 265-nm fast channel. As this would have led to inaccuracies in our results, we opted to go for a conventional pump-probe method for these two wavelengths. At an excitation wavelength of 230 nm, the multiphoton background arising from the 257-nm UV laser overlap with the IR overwhelmed the signal, producing very noisy data. To prevent that, we again chose to use the pump-probe technique. The 243-nm probe laser contributed to less multiphoton background and the single probe pulse allowed us to offset the probe laser in time.

Refer to Point iii for additional information regarding our choice of the two techniques.

Changes to the manuscript
The benefits of the Doppler-free technique are now outlined more clearly in the experimental section of the manuscript (Pages 5-6).

Referee: 2

Comments to the Author
The authors report on experimental and theoretical studies of the dynamic Stark effect in the DJ photodissociation reaction.

The observed changes in the branching ratio are significant for dissociation in the range 230 – 265 nm, but less obvious outside this range. The theoretical simulations use one-dimensional wavepacket propagation with a simplified model, in particular concerning the guesses made for the Stark shifts. Nevertheless, this is a very interesting observation that should be communicated to stimulate discussion. Below I list a few questions that the autors might consider in the final version:

i. The intensity of the laser providing the Stark field is given in Watt throughout the paper, but this is the average power of a pulsed laser. In order to translate this into the true intensity at the moment of the dissociation one needs the additional information about the pulse duration and the repetition rate. The peak intensity of the pulses would be more informative.

We agree. Thank you for drawing this to our attention.

Changes to the manuscript
We have added and replaced the peak powers (Watts) with peak intensities (W/cm^2) in the figure captions and legends, as well as in several places in the text of the manuscript (page 2, 5, 9, 14).

ii. A change in the branching ratio is interpreted as in increase of the reaction velocity of one of the reaction channels. However, a slowing of the other channel could also explain the experimental observation. The interpretation in terms of a "photon catalysis" can, however, only be applied in the first case. Can one exclude the second possibility?

We observe no changes in the product speeds with application of the strong, nonresonant field. Instead, a change in the branching ratio is interpreted as a change in the relative populations of the "slow" and "fast" channels at these distinct speeds.

Please consider that the total product yield of this reaction always equals a constant, and there are two channels that contribute to that yield. By necessity, the enhancement of one product channel occurs with a reduction in the other channel. Conversely, the inhibition of one channel is observed alongside the enhancement of the other channel. As the reviewer suggests, it is not possible to disentangle these two conditions from one another. Instead, we consider two rate constants for two processes and measure the relative change. Our use of the term "photon catalysis" or "laser field catalysis" for this system is in accordance with literature precedent established by Stolow and coworkers (Reference 1,2) in their study on the photodissociation of the similar system, IBr, in the presence of a strong nonresonant field. In this work, they interpret a change in the branching ratio as evidence of laser field catalysis, where one channel is enhanced/ catalyzed *relative* to another through modification of potential energy surfaces.

Changes to the manuscript
We have now added an explicit mention that Stolow and coworkers defined this as "catalysis" in the manuscript on page 2. Additionally, we have clarified the changes to be relative to each other on page 1 and 9.

iii. The usual interpretation of catalysis includes the lowering of a reaction barrier. The energy profiles along the reaction coordinate shown in figure 1 seem to be purely repulsive. How could one understand a barrier in this case? How about the alternative interpretation: That the Stark field results in a kind of trapping of the system that differs in efficiency for the two reaction channels?

We use the term "photon catalysis" or "laser field catalysis" in accordance with literature precedent established by Albert Stolow in his work on the photodissociation of IBr (Reference 1), a molecule that also exhibits prompt dissociation from nearly purely repulsive surfaces. For these two similar systems, we do not consider the nonresonant field to be catalyzing the reaction by lowering an energy barrier which exists along any one excited potential surface. Rather, we understand the IR field to be catalyzing one reaction pathway by enhancing its rate relative to the others, without being consumed, through Stark shifting of potential energy surfaces. For the adiabatic transitions involved in this dissociation, a red-shifting of the branching ratio curve occurs. In a sense, a figurative barrier is lowered which allows for the observation of dissociation dynamics at lower excitation energies than they are observed in the absence of the field. In other words, less excitation energy is required to achieve the same result. Furthermore, by changing the position of the crossings, the IR-field facilitates nonadiabatic transitions that enhance/catalyze the production of the I* channel at 230 nm.

We hesitate to explain these results in terms of "trapping" of the system because this might imply electric-field-induced energy wells instead of purely repulsive surfaces.

Changes to the manuscript
We have rephrased the wording in our explanations in the manuscript (Page 1, 2, 3) to make more clear that catalysis here is defined in accordance with Stolow's work on the IBr system (Reference 1, 2) and that no energy barrier on a single excited state surface is lowered. Instead, nonresonant photons catalyze the reaction by facilitating one pathway relative to another, without being used up or changed.

We hope that with these changes our manuscript is ready for publication.

Photon catalysis of deuterium iodide photodissociation

Kallie I. Hilsabeck [†a], Jana L. Meiser [†a], Mahima Sneha [†a], N. Balakrishnan[b], Richard N. Zare[a*]

[a] Department of Chemistry, Stanford University,
Stanford, CA, 94305, USA
[b] Department of Chemistry and Biochemistry, University of Nevada, Las Vegas,
Las Vegas, NV, 89154, USA

[†] These authors contributed equally to this research.

All correspondence should be addressed to rnz@stanford.edu.

A catalyst enhances a reaction pathway without itself being consumed or changed. Recently, there has been growing interest in the concept of "photon catalysis" in which nonresonant photons, which are neither absorbed nor scattered, promote reactions. The driving force behind this effect is the interaction between the strong electric field associated with a pulsed, focused laser and the polarizability of the reacting system. In this study, the effect of near-infrared, nonresonant radiation on the photodissociation of deuterium iodide is demonstrated. We use nanosecond pulses rather than time-resolved spectroscopy to investigate the average effect of the electric field on the branching ratio for forming D + I($^2P_{3/2}$) and D + I($^2P_{1/2}$). Changes in the measured D-atom speeds between field-free and strong-field conditions confirm substantial differences in dissociation dynamics. Both the magnitude and direction of change in the branching ratios are dependent upon the photodissociation wavelength. Experiments and theoretical calculations confirm that the mechanism for photon catalysis under these conditions is dynamic Stark shifting of potential energy surfaces rather than electric-field-induced alignment of reagent molecules.

I. Introduction

Chemists strive to achieve control over chemical reactions by manipulating such physical variables as pressure, temperature, solvent polarity, and reagent concentration; however, even thermodynamically favored reactions often resist yielding appreciable amounts of product because the kinetics are too slow. The key to unlocking such reactions is to find a suitable catalyst, a species that enhances the rate of a reaction without itself being used up or changed.

Catalysis is a vast and quickly developing area in chemical research with applications in several fields of science and technology. Standard examples of chemical catalysts include enzymes, organometallic complexes, and metal surfaces. Although very different in structure, each of these substances share a common function: through electric fields, they interface with specific bonds or functional groups within a reacting compound.[1, 2] The result of this action is to lower the energy of the transition state for a specific reaction pathway relative to others, thus enhancing its reaction rate. Applying electric forces[3] to reacting molecular systems can be achieved even in the absence of a traditional chemical catalyst, for example, through the application of a focused laser pulse.

Light exists as a propagating wave of electric and magnetic fields. For decades, the interaction of light with matter has been used to induce spectroscopic transitions through the resonant excitation of molecules to rotational, vibrational, and electronic excited states. The effect of nonresonant radiation is often considered to be insignificant and disregarded; however, this assumption is only valid in the limit of a "weak" field.[2] With pulsed lasers, it is possible to achieve electric field strengths that exceed by orders of magnitude the static field strengths supplied by common high-voltage power supplies. For

example, an IR laser pulse (1064 nm) of 4 W focused to a beam waist radius of 30 μm and having a duration of 10-11 ns, has a peak intensity of 3.4×10^{12} W/cm^2 and electric field strength, ε_0, on the order of 5.0×10^7 V/cm. At these high laser powers, nonresonant radiation, through its electric field, can influence the course of a reaction by interacting with the molecular system's polarizability α to lower an activation barrier directly. Because there is no net consumption of photons in this process, the photons behave as catalysts rather than reactants in a process referred to as photon catalysis, or laser field catalysis as it was first defined by Stolow and coworkers.[1, 2, 4, 5]

To elaborate, consider a simple collinear molecular system, e.g., the photodissociation of a linear molecule. For frequencies much greater than the reciprocal of the laser pulse duration, the Hamiltonian can be written in the following way:

$$\bar{\mathrm{H}} = H_0 + BJ^2 - \frac{1}{4}\varepsilon_0^2\left[\alpha_\perp + (\alpha_\parallel - \alpha_\perp)\cos^2\theta\right], \quad (1)$$

where $H_0 + BJ^2$ describes a rotating molecular system in the absence of an external field, ε_0 is the electric field strength, θ is the angle between the electric field and the molecular axis, and $\alpha_\parallel$ and $\alpha_\perp$ represent the polarizabilities of the linear system, parallel and perpendicular to the molecular axis.[6] Please note that possible interaction with a permanent dipole moment averages to zero and therefore is not included. The term in square brackets in this equation clearly outlines two possible effects of a strong, nonresonant electric field on a molecular system:

1) *Stark shift of energy levels* - The bracketed terms that are independent of θ result in a Stark shift of the molecule's potential energy surfaces. The distortion of these surfaces may alter adiabatic and/or nonadiabatic dissociation dynamics by impacting the intersection geometry and Landau-Zener hopping probabilities, thereby enhancing or depleting the contribution from the available channels to the total product yield.
2) *Alignment* - The term involving $\cos^2\theta$ mixes rotational levels, causing the molecular system to become aligned in the presence of a strong electric field. This behavior is most prevalent for atoms/molecules in the ground rotational state. The effect of alignment on the dissociation dynamics is dependent upon the anisotropy of the dissociation and the polarization of the strong electric field.

Hydrogen halide and dihalide molecules provide model theoretical[7-14] and experimental[15-23] systems for photodissociation reactions involving an excitation from the ground state to an electronically excited potential energy surface. Because they are well-characterized in the literature and exhibit significant polarizability even in the ground state, these simple molecules are also excellent starting points for the experimental demonstration of photon catalysis. To date, the most well-known observation of photon catalysis involved the photodissociation dynamics of IBr, a dihalide molecule. Stolow and coworkers[1] used time-resolved, ultrafast spectroscopy to confirm that application of a strong, nonresonant infrared (IR) field (λ = 800 nm) led to substantial changes in the relative contributions of two competing IBr dissociation channels. This study demonstrated one of the possible effects of strong, nonresonant radiation on a molecular system: dynamic Stark shifting of potential energy surfaces to energetically favor the formation of one product over another. For this system, with nearly purely repulsive excited state surfaces, the nonresonant field did not catalyze the reaction by lowering an energy barrier along any one excited potential surface. Instead, the IR field catalyzed one reaction pathway by enhancing its rate relative to another, without being consumed, through Stark shifting of potential energy surfaces. Another study by Bañares and coworkers[4] demonstrated that the presence of an ultrafast strong laser field gives rise to light induced conical intersections in the CH_3I

potentials, leading to a substantial change in the branching ratio of different product channels in the photolysis of this molecule.

It has also been experimentally observed that a second effect, alignment of reagent molecules by a nonresonant laser field, can lead to a change in the contribution of different channels to the overall product yield. Stapelfeldt *et al.*[24] demonstrated control over the ratio between two photodissociation channels of iodine (I_2) through application of a strong, near-IR laser pulse polarized either parallel or perpendicular to the polarization axis of the excitation laser pulse. This result is consistent with the anisotropic nature of the photodissociation: the two major product channels are related adiabatically to two different excited potential energy surfaces that are accessed through either a parallel or perpendicular transition, respectively. Therefore, one of the product channels is favored when the aligning and dissociating laser pulses are polarized in the same direction, and the other channel is favored when the two lasers are polarized perpendicularly to each other. Similar studies involving linear molecules like OCS (Sakai *et al.*[25]), as well as more complex compounds like pyrimidine (Franks *et al.* [26]), also have shown that it is possible to control a molecule's alignment using a strong electric field.

In the work presented here, we studied the impact of the two aforementioned effects of a strong, nonresonant, near-IR field on photodissociation of deuterium iodide (DI). As in the case of IBr, DI exhibits prompt dissociation from nearly purely repulsive surfaces. Two channels arise from the spin-orbit interactions in the iodine atom.[7-10, 15-20] The spin-orbit excited state of the I atom ($^2P_{1/2}$) is higher in energy than the ground state I atom ($^2P_{3/2}$) by 0.94 eV. Therefore, the dissociation channel D + I($^2P_{3/2}$), where the I is in its ground state, has higher kinetic energy disposed in the corresponding D atom and is known as the fast channel. The slow channel corresponds to the spin-orbit excited state of iodine, I($^2P/_{1/2}$), which hereafter will be denoted by I^*. By the necessity that total energy be conserved, this channel has slower-moving D atoms. The extent to which each channel is populated depends upon the potential energy curve to which the molecule is initially excited (i.e., the energy of the exciting photon), and the probability for nonadiabatic transitions within the Franck-Condon region (Fig. 1). The ratio of the respective reaction cross sections, σ, of the slow channel to the fast channel is referred to as the branching ratio, $\sigma[I^*]/\sigma[I]$. The wavelength dependence of the branching ratio in the absence of a strong electric field has previously been characterized, and is observed to peak approximately at 250 nm.[15] By monitoring changes in the branching ratio with application of strong, nonresonant radiation, experimental results provided insight into the photon-catalyzed process.

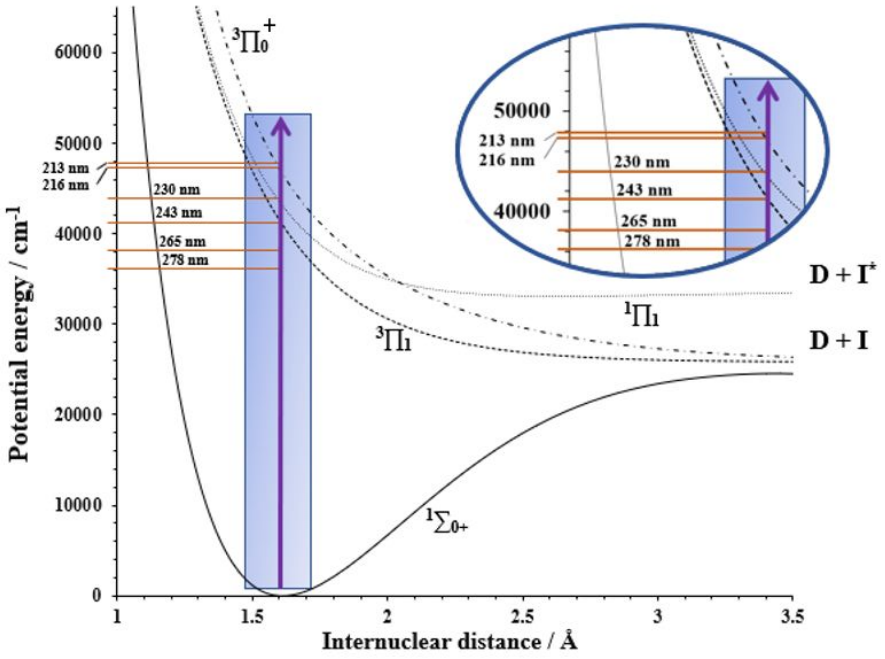

Fig. 1 Potential energy curves for the ground and low-lying excited electronic states of DI involved in one-photon dissociation. The parts of the potential that were sampled at each experimental excitation wavelength, within the Franck-Condon region, are illustrated schematically.

Simple theoretical calculations that model the effect of dynamic Stark shifting on the branching ratio were performed to complement and qualitatively support experimental results. The photodissociation dynamics were treated using the time-dependent wave packet formalism. Details of the field-free dynamics are given in prior works.[7-9] Although the photodissociation dynamics of HI in the presence of two-color, intense laser pulses has been reported previously,[27] the effect of a pulsed, nonresonant electric field on the dissociation dynamics and the I*/I branching ratio has not been theoretically explored. Below, we provide a brief description of the theoretical approach, following the methods given in Refs. 9 and 27.

The time-dependent Schrödinger equation was solved to describe the photodissociation dynamics of DI in the A band. Five electronic states were considered in the study: $X^1\Sigma^+$, $^3\Pi_1$, $^1\Pi_1$, $^3\Pi_{0^+}$, and $t^3\Sigma_1^+$, denoted $V_i(R)$, i = 1-5. The Schrödinger equation may be written as

$$i\hbar\frac{\partial\mathbf{\Psi}(R,t)}{\partial t} = \left[-\frac{\hbar^2}{2m}\boldsymbol{I}\frac{d^2}{dR^2} + \boldsymbol{U}(R)\right]\mathbf{\Psi}(R,t), \quad (2)$$

where $\mathbf{\Psi}$ is a column vector of wave functions with components ψ_i, $i = 1-5$, for the five electronic states, $\boldsymbol{I}$ is a 5×5 identity matrix, and $\boldsymbol{U}(R)$ is a 5×5 potential energy matrix with the diagonal elements,

$$U_i(R) = V_i(R) - \frac{1}{4}\alpha_i(R)\varepsilon_0(t)^2. \quad (3)$$

The second term of Eq. (3) denotes the Stark-shift of the potential curves due to the electric field. Rotational effects were ignored in our calculations, and the polarizability term was approximated by its

parallel component, with values taken from Maroulis[28] for the $X^1\Sigma^+$ state. The anisotropy of the polarizability is quite small for the ground state of HI, $\Delta\alpha = \alpha_{\parallel} - \alpha_{\perp} = 2.94$ au, compared to the parallel component, $\alpha_{\parallel} = 37.98$ au, at the equilibrium internuclear separation. The Stark shift was applied only to the excited state potential curves ($V_i(R)$, i = 2-5).

Alignment, the second possible effect of a nonresonant field, is also investigated experimentally. The studies on HI photodissociation by Langford *et al.*[15], and DI dissociation by Heck and Chandler[29] show that independent of wavelength of excitation, the fast and slow channels for both HI and DI result predominantly from adiabatic perpendicular and parallel transitions, respectively. Therefore, changing the relative polarizations of the near-IR pulse and exciting pulses allows for the deconvolution of the effects of Stark shifting and alignment on reaction outcome. This study is further distinguished from previous work because nanosecond pulses are employed to supply the field, which are much longer than the timescale of the reaction. This presents an opportunity to determine the more general effect that a nonresonant electric field had on modifying total reaction yield, rather than doing a time-resolved study. It is also more conducive to future extension of the effect beyond unimolecular reactions, e.g., to bimolecular reactions such as DI + D $\longrightarrow$ D_2 (v', j') + I.[30, 31]

II. Methods

Experimental Details

A detailed description of the experimental setup has been provided in previous publications.[32] For this set of experiments, a mixture of 5% DI (D 98%, Cambridge Isotopes Laboratories, Inc.) in an inert carrier gas (Ar, He) was expanded supersonically into a vacuum chamber through a pulsed valve (General Valve, Series 9) at a stagnation pressure of 10-15 psi. We observed no significant differences in the branching ratios using different carrier gases. The molecular beam was collimated through a 2 mm skimmer and intersected orthogonally by focused photolysis and photoionization (probe) lasers, as well as the IR laser (1064 nm) that supplied the strong electric field. Resulting positively charged D^+ ions were accelerated through a Wiley-McLaren time-of-flight (TOF) mass spectrometer and collected on a position-sensitive delay-line detector. Time and position information were used to extract lab-frame speed distributions for the product D^+ ions. The branching ratios were calculated by integrating the relative areas under the slow and fast channel peaks in the speed distributions.

DI photodissociation was carried out at six wavelengths in the A-band between 213 and 278 nm, both with and without the strong electric field supplied by the near-IR laser. Under each set of conditions, three to five reproducible data sets, averaging over 3000-4000 ions, were collected. For each experiment, the photolysis laser power was maintained at approximately 10-20 μJ. The D-atom product was ionized using (2+1) resonance enhanced multiphoton ionization (REMPI) via the 2s – 1s transition at approximately 243 nm. Under the application of the strong electric field, the REMPI line was red-shifted 10 - 20 pm to account for the observed Stark shift of the D-atom signal. A probe laser power of 5 μJ was sufficient for this experimental setup. The average power peak intensity of the IR laser was maintained between 3.4×10^{12} W/cm^2 and 5.1×10^{12} W/cm^2, which, when focused with a lens of f = 35 cm, corresponds to an electric field strength of approximately 5.1×10^7 V/cm to 6.3×10^7 V/cm in the interaction volume. Low powers of the UV lasers ensured that the strong electric field was solely produced by the IR laser. A detailed description of the method of background subtraction is provided in the supplementary information (Fig. S1).

Two techniques were used for D-atom detection. For excitation wavelengths of 213 nm, 216 nm, 243 nm, and 278 nm, the Doppler-free technique was implemented. Two counterpropagating UV lasers were overlapped spatially and temporally, and their wavelengths were chosen such that

combined they achieved resonance with the (2+1)-REMPI line at 243 nm. The dissociation laser was set at higher power so that it solely photolyzed the DI molecule. Minimal photolysis contamination from the other UV laser was subtracted as background. Because both lasers contributed to the probe step and were traveling in opposite directions toward the interaction region, D atoms were ionized regardless of their speed with respect to the laser propagation direction. This condition strongly increased the signal without impacting the amount of background in our experiments. Furthermore, as the Doppler-free technique removed the requirement to perform a scan over the Doppler range, it reduced inconsistencies arising from power and overlap fluctuations of the lasers throughout data collection and produced speed distributions with a more Gaussian shape.

For 265 nm and 230 nm excitation, a traditional pump-probe setup was used. DI molecules were first dissociated by the pump laser and, after a short time delay of 3 ns, the resulting D-atom product was ionized using (2+1)-REMPI via the 2s – 1s transition at approximately 243 nm. The probe laser wavelength was scanned over the Doppler range. This detection technique was chosen for these two wavelengths because the complementary UV wavelength required to fulfill the Doppler-free condition either produced strongly overlapping peaks in the speed distribution (265 nm, Fig.S2) or caused an overwhelming amount of multiphoton background with the IR (230 nm).

The ultraviolet laser light of appropriate wavelengths for the photolysis and photoionization processes was attained in two ways: frequency tripling the output of a dye laser (Lambda Physik, LPD 3000) pumped by the second harmonic of an Nd:YAG^{3+} laser (Spectra Physics, GCR Series), or frequency doubling the output of a dye laser (Lambda Physik, LPD 3000) pumped by the third harmonic of an Nd:YAG^{3+} laser (Quanta-Ray, DCR-3). The strong electric field was supplied by the fundamental of a third Nd:YAG^{3+} laser (Spectra Physics, GCR Series) at 1064 nm. All frequency mixing was achieved using BBO crystals.

Computational Details

Theoretical calculations correspond to a pulse width of τ = 500 fs. Although we used a much longer IR pulse for our experiments, the probability for excitation and dissociation from each excited potential surface reached a steady state within about 50 fs, by which time the electric field also had reached 97% of its peak value (Fig. S3). Therefore, this approximation is reasonable for comparison with our experimental results.

In the absence of any literature results on the polarizabilities of HI for the various excited electronic states considered here, we have approximated the excited state polarizabilities, α_i(R)= α_1(R)×*f(i), i* = 2-5, where α_1(R) is the polarizability of the ground state and *f(i)*, *i* = 2-5 are scaling factors for the excited state polarizabilities. We have taken wide latitude in choosing the scaling factors to explore any unusually large effect induced by the electric field. Different sets of calculations were performed with different values of the scaling parameters to examine the sensitivity of results to the shift in the excited state potentials induced by the electric field. Five different sets of calculations were performed for a given laser intensity with the excited state polarizabilities varied by a factor of 1.2 to a factor of 15. They are listed below as Shift 1 through Shift 5:

Shift1: $f(2) = 1.2, f(3) = 1.3, f(4) = 1.5, f(5) = 1.5$
Shift2: $f(2) = 2.0, f(3) = 2.5, f(4) = 3.0, f(5) = 3.0$
Shift3: $f(2) = 3.0, f(3) = 3.5, f(4) = 4.0, f(5) = 4.0$
Shift4: $f(2) = 4.0, f(3) = 4.5, f(4) = 5.0, f(5) = 5.0$
Shift5: $f(2) = 10.0, f(3) = 11.0, f(4) = 15.0, f(5) = 15.0$

In each case, $f(4)$ and $f(5)$ were assumed to be the same, as excited state 5 does not contribute appreciably to the one-photon dissociation process in the wavelength range reported here. Although

this choice of scaling factors is rather arbitrary, large variations in excited state polarizabilities with factors from 2-6 have been reported for diatomic molecules such as LiH and NaH.[33] Preliminary ab initio calculations without the inclusion of spin-orbit coupling also suggest a factor of 2 or higher values for the excited state polarizabilities with strong anisotropic components. Table S1 presents details of this calculation in the supplementary information.

The off-diagonal elements $U_{1i}(R) = U_{i1}(R)$, i = 2-5 of $\boldsymbol{U}(R)$ denote the field-induced couplings, which in the dipole approximation are given by $U_{1i}(R) = -\mu_{1,i}(R)\varepsilon_0(t)\cos(\omega t)$, i = 2-5 where $\mu_{1,i}(R)$ are the R-dependent transition dipole moments between the ground state and the excited electronic states, i = 2-5. The electric field is defined as $\varepsilon_0(t) = \varepsilon_0 g(t)$, where ε_0 is the peak field strength, and the envelope function g(t) is taken to be a Gaussian centered at t = 0, $g(t) = \exp[-4\ln(2)t^2/\tau^2]$ with full-width τ at half-maximum.

The excited-state potential curves and transition dipole moments are taken from Camden *et al.*,[34] which provide experimentally calibrated parameters. We used parameters corresponding to model 1 in Table 3 of Camden *et al.*[34] The branching ratio is very sensitive to the slope of the excited state potential curves in the Franck-Condon region, and the potential curves and dipole moment functions of model 1 yield better agreement with experiment than the ab initio potential curves and transition dipole moments of Alekseyev *et al.*[35] However, Alekseyev *et al.*[36] have also argued that a slight upward shift of approximately 500 cm^{-1} of the ab initio computed excited triplet potential curves and a 5% increase in the $(^1\Pi_1, ^3\Pi_1)\leftarrow X$ transition dipole moments yield results in close agreement with experiment, an analysis that also favors model 1 parameters. For the ground $X^1\Sigma^+$ state, we used the potential energy curve of Coxon and Hajigeorgiou[37] in the short-range and merged it smoothly with the ab initio potential of Alekseyev *et al.*[35] for R > 6.3 bohr. We have also included the spin-rotation coupling between the $^1\Pi_1$ and $^3\Pi_{0^+}$ states as an off-diagonal matrix element $U_{34}(R) = U_{43}(R)$, but this has a negligible effect on the branching ratio as found for field-free dynamics in Ref. 9. Although we have included the $t^3\Sigma_1^+$ electronic state correlating with I* channel in our calculations, its effect is not important and it does not contribute to I* channel at the excitation wavelengths considered in this work.

The Schrödinger equation was solved using the split-operator method[38] with appropriate absorbing boundary conditions.[39] The wave packet was initialized as $\psi_1(R,t=0) = \phi_{v=0,j=0}(R)$, $\psi_i(R,t=0) = 0, i = 2-5$, where $\phi_{v=0,j=0}(R)$ is the rovibrational ground state wave function of the $X^1\Sigma^+$ state. A radial grid of 512 points in the range R = 2-20 au was used to discretize the wave packet. See Ref. 9 for more details. Diagonalization of the potential matrix at each time step of the propagation yielded an adiabatic "light-induced" potential.

II. Results & Discussions

Deuterium iodide was photodissociated under field-free conditions and in the presence of the strong electric AC field supplied by a nonresonant, near-IR laser pulse at 1064 nm. Figures 2a-2f present the measured D-atom speed distributions for six excitation wavelengths spanning the A band: Fig. 2a at 213 nm, Fig. 2b at 216 nm, Fig. 2c at 230 nm, Fig. 2d at 265 nm, Fig. 2e at 243 nm, and Fig. 2f at 278 nm. Table S2 lists the fast and slow D-atom speeds for the excitation wavelengths used in this study. For these sets of experiments, the excitation laser pulse was polarized vertically, and the IR laser pulse was polarized horizontally.

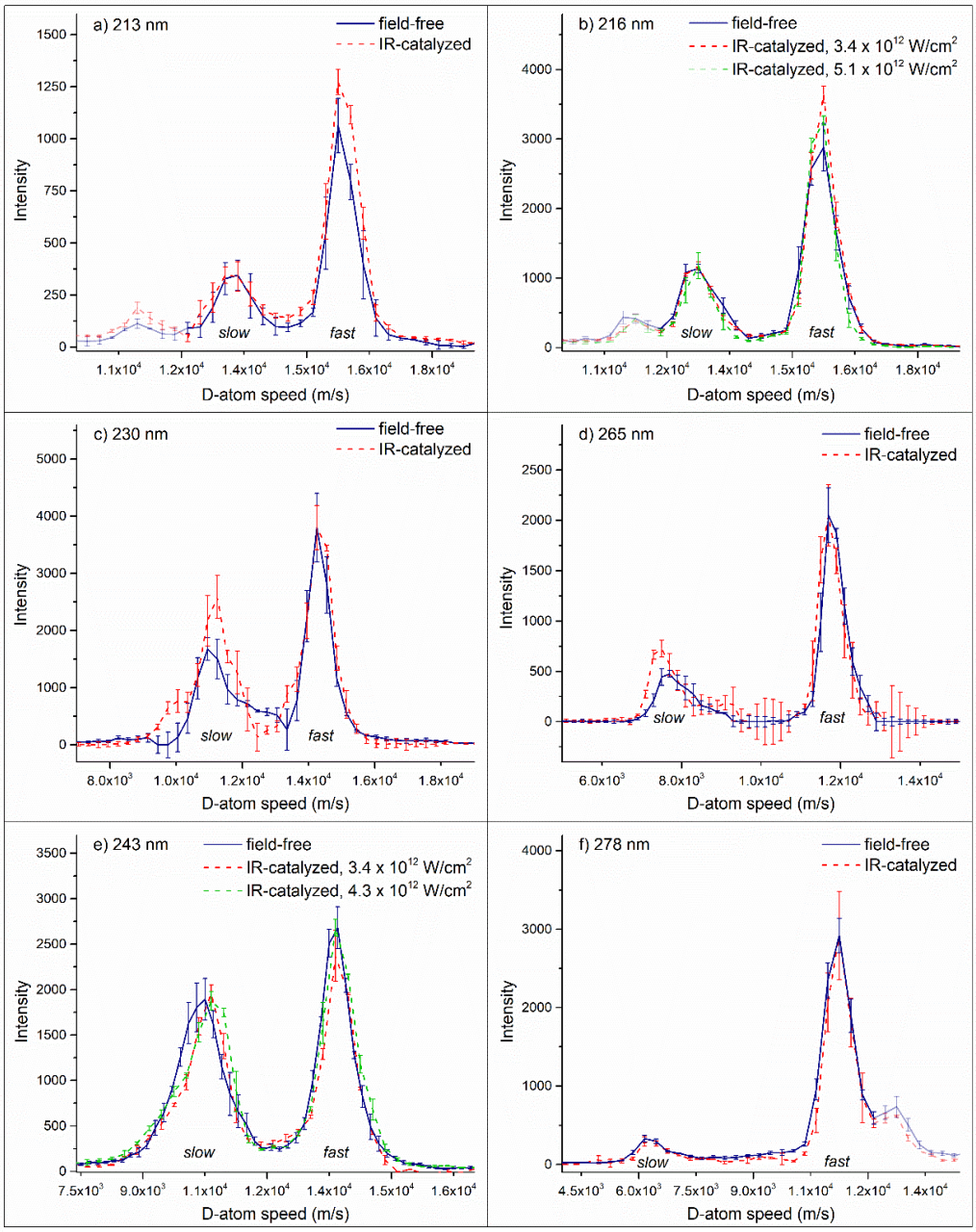
a) 213 nm
field-free
IR-catalyzed
b) 216 nm
field-free
IR-catalyzed, 3.4 x 10^12 W/cm^2
IR-catalyzed, 5.1 x 10^12 W/cm^2
c) 230 nm
field-free
IR-catalyzed
d) 265 nm
field-free
IR-catalyzed
e) 243 nm
field-free
IR-catalyzed, 3.4 x 10^12 W/cm^2
IR-catalyzed, 4.3 x 10^12 W/cm^2
f) 278 nm
field-free
IR-catalyzed
Intensity
D-atom speed (m/s)
slow
fast

Fig. 2 D-atom speed distributions for the photodissociation of DI at a series of excitation wavelengths: a) 213 nm, b) 216 nm, c) 230 nm, d) 265 nm, e) 243 nm, and f) 278 nm. The blue lines represent data collected in the absence of a strong electric field (field-free), and the red dashed lines represent data collected at an IR peak intensity of 3.4×10^{12} W/cm^2 ($\varepsilon_0 = 5.1 \times 10^7$ V/cm, IR-catalyzed). The green dashed lines in b) and e) are for experiments performed at higher IR peak intensities of 4.3×10^{12} W/cm^2 and 5.1×10^{12} W/cm^2, respectively ($\varepsilon_0 = 5.8 \times 10^7$ V/cm, and 6.3×10^7 V/cm). Error bars denote one standard deviation over 3-5 experimental data sets. A third peak is observed in the case of Fig. 2a, 2b, and 2f, here marked in a lighter shade for clarity, which originates from photolysis by the complementary Doppler-free probe laser. The shoulders on the leading edges of the fast and slow channel peaks in Fig. 2c are also consistent with 243-nm dissociation by the probe laser.

The experimental branching ratios under field-free conditions were in reasonable agreement with previously published values.[15] Upon application of a strong AC field that encompassed the entire photodissociation process, we observed significant changes in the branching ratios to one standard deviation. These experimental findings provide clear evidence of the measurable effect of a nonresonant IR field on the photodissociation dynamics of DI. Furthermore, because IR photons were neither absorbed nor changed during this process, they acted as catalysts to selectively lower activation barriers for one pathway relative to another.

Both the magnitude and direction of this change were dependent upon the excitation energy. At 213 nm and 216 nm (Fig. 2a and 2b), the branching ratio decreased by 23% and 14%, respectively, under strong field conditions, suggesting that the *fast* product channel was enhanced relative to the slow channel by the application of the IR field in this wavelength range. Conversely, at 230 nm and 265 nm (Fig. 2c and 2d), the branching ratio increased significantly by 36% and 39%, respectively, which indicates a relative increase in the *slow* channel contribution with application of the IR field. No measurable change in the branching ratio was perceived for photodissociation at 243 nm or 278 nm (Fig. 2e and 2f). Higher intensity IR experiments were performed for excitation at 216 nm and 243 nm. As is evident from Fig. 2b and 2e, this increase in electric field strength was not sufficient to produce a measurable change from the branching ratio at the lower IR power. Table 1 summarizes the results.

Table 1 Experimentally measured branching ratios for the photodissociation of DI in the presence and absence of a strong, nonresonant IR field. Uncertainties represent one standard deviation over 3-5 experimental data sets.

Excitation Wavelength (nm)	IR Field-free Branching Ratio	Branching Ratio for IR Peak Intensity = 3.4×10^{12} W/cm^2 ($\varepsilon_0 = 5.1 \times 10^7$ V/cm)[a]
213	0.52 ±0.02	0.40 ±0.02
216	0.50 ±0.02	0.43 ±0.02
230	0.67 ±0.08	0.91 ±0.08
243	1.01 ±0.04	1.00 ±0.03
265	0.31 ±0.04	0.43 ±0.02
278 (H)[b]	0.13 ±0.01	0.12 ±0.01
278 (V)[b]	0.13 ±0.01	0.12±0.01

[a]For 243-nm and 216-nm excitation, IR experiments were also performed at $\varepsilon_0 = 5.8 \times 10^7$ V/cm and 6.3×10^7 V/cm, but there were no measurable changes from the branching ratio at 5.1×10^7 V/cm.
[b]For 278-nm excitation, data were collected with the IR laser polarized horizontally (H) and vertically (V).

A third peak was observed in the case of Fig. 2a, 2b and 2f. As mentioned previously, the Doppler-free probing technique used for these excitation wavelengths involved two counterpropagating lasers that can each contribute to photolysis. These additional peaks were the result of a small amount of DI photolysis by the other UV laser, which could not be fully accounted for in the background subtraction. However, as these peaks were well-separated from the slow and fast channels resulting from the excitation wavelength, they did not interfere with branching ratio determination. Similarly, small shoulders on the leading edges of the slow and fast channel peaks in Fig. 2c corresponded to 243-nm dissociation by the probe laser. Shoulders were not included in the area that was integrated for the branching ratio calculations; however, inclusion of the shoulder for both the slow and fast channel peaks did not cause the branching ratio to fall outside of the currently reported uncertainty because the branching ratio at 243 nm was approximately equal to 1 for both the field-free and IR-field cases.

It should also be noted that the two excitation wavelengths for which an increase in the slow channel were observed, 230 nm and 265 nm, were also the two wavelengths that employed the pump-probe approach. To confirm that this result was not caused by a systematic bias introduced by the detection technique, the experiments at 243-nm excitation were repeated using a one-laser, pump-probe approach. With both the Doppler-free and pump-probe techniques, the same result was observed: no change in branching ratio was detected with application of the strong field (Fig. S4a and S4b). Furthermore, the experiments at 230 nm were repeated with a 0 ns delay instead of 3 ns to ensure that the enhancement in the slow channel was not artificially created because of the faster moving atoms escaping the interaction volume before ionization. Measured speed distributions and branching ratios were not influenced by a time delay of this magnitude, under either field-free or IR-field conditions. Collectively, these results indicate that no systematic bias existed in our detection setup.

Degree of Alignment

Because the slow and fast channels correspond predominately to parallel and perpendicular transitions, respectively, alignment of reactant molecules with the electric field should favor one channel over the other, resulting in products with different branching ratios. In the experiments presented to this point, the excitation laser and IR laser were polarized perpendicularly to one another, and any significant alignment would have favored the formation of faster-moving D atoms. To evaluate the extent of alignment in the beam, we repeated the experiments at an excitation wavelength of 278 nm with a vertical polarization of the IR beam, parallel to the polarization of the excitation laser pulse (Fig. 3).

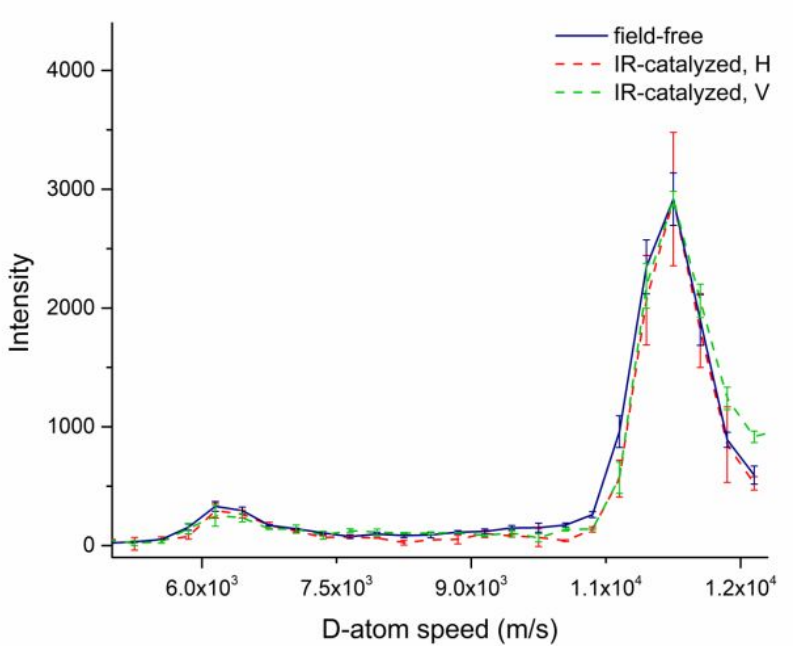

Fig. 3 D-atom speed distributions for the photodissociation of DI at 278 nm in the absence (blue line) and presence of vertically polarized (red dashed line) and horizontally polarized (green dashed line) IR field. Error bars denote one standard deviation over 3-5 experimental data sets.

As Fig. 3 and Table 1 indicate, the branching ratio in the presence of the strong field was independent of the polarization of the IR laser pulse relative to that of the excitation laser pulse at an excitation wavelength of 278 nm. Calculations predict that most of the alignment should occur for molecules in the ground rotational state, J = 0.[40] To determine the percentage of molecules present in the ground rotational state, the rotational distribution of DI in the molecular beam was measured. A large iodide ion background signal at the desired wavelengths precluded a quantitative measurement; however, qualitatively it was confirmed that there were roughly five times more molecules in the J = 1 level than in the J = 0 level, and that a discernable DI signal existed for rotational levels up to J = 10. Figure S5 in the SI displays an approximation for the rotational distribution of DI in our molecular beam. As the majority of the DI molecules in the molecular beam have non-zero rotational energy ($J \neq 0$), this result is consistent with no detectable alignment by an external electric field at an excitation wavelength of 278 nm (Fig. 3). This result is general, as alignment is not expected to be wavelength-dependent. The negligible impact of alignment under these experimental conditions suggests that the observed photon catalysis effect arose primarily because of the dynamic Stark shifting of potential energy surfaces, rather than electric-field-induced alignment.

Dynamic Stark-shifting of Potential Surfaces

Theoretical calculations were performed to make a qualitative prediction about how the dynamic Stark shifting of potential energy surfaces is expected to impact the relative contributions of the slow and fast channels to the dissociation of DI. Excited state polarizabilities were scaled up from the ground state over a range of scaling factors, as described above, to give an estimate of the expected Stark shifts. At an electric field strength of 5.1×10^7 V/cm, shifts 1-4, corresponding to different scaling factors, yielded comparable results. Conversely, shift 5 displayed an entirely different behavior that suggests that the scaled polarizabilities used were unrealistically large. This result is reflected in the

shifted potential energy curves and branching ratios presented in Fig. 4 and 5. In moving forward with the discussion, we take shift 2 as an acceptable approximation for the excited state polarizabilities.

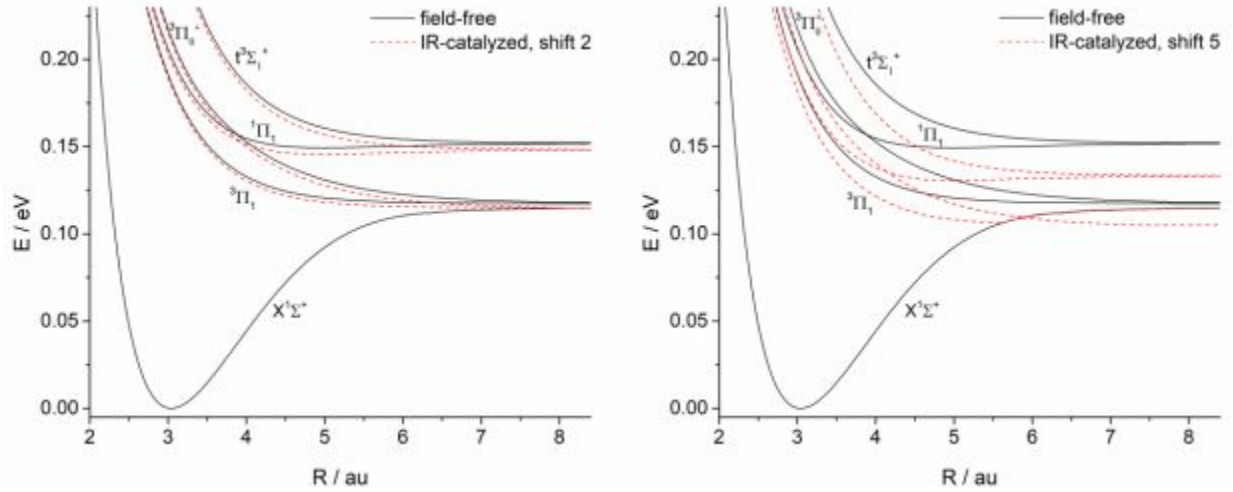

Fig. 4 Potential energy curves for the one-photon dissociation of DI under field-free (black, solid) and IR-catalyzed (red, dashed) conditions using the polarizabilities of a) shift 2 and b) shift 5. The electric field strength for these calculations was 5.1×10^7 V/cm.

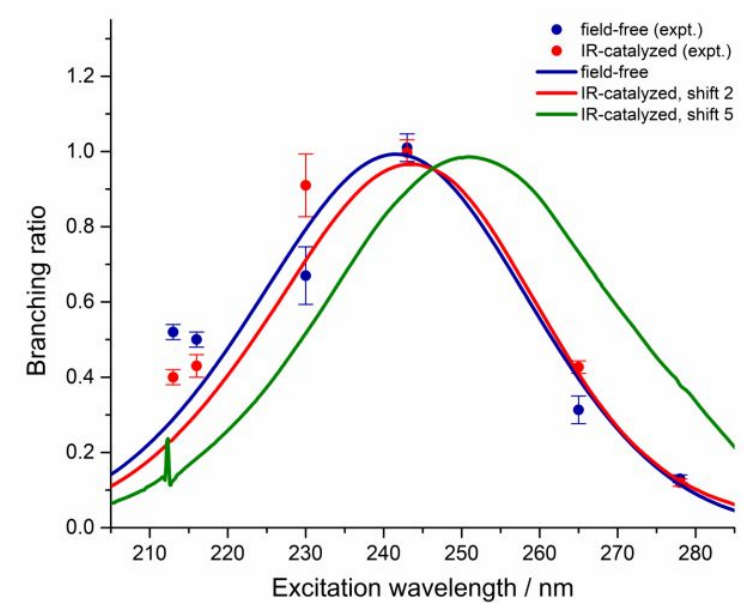

Fig. 5 Experimentally and theoretically determined branching ratios for the photolysis of DI, both in the presence (red and green) and absence (blue) of the strong IR field at 5.1×10^7 V/cm. Results of calculations for shifts 2 (red) and 5 (green) are displayed. Error bars denote one standard deviation over 3-5 experimental data sets.

Comparison of the experimental and theoretical data, presented in Fig. 5, clearly shows that the theory cannot quantitatively describe this system or the effect of the nonresonant IR field on its dynamics. However, theoretical calculations do provide qualitative insight into the photon-catalyzed

process. The predicted effect of the nonresonant field is to shift the excited potentials to lower energies (Fig. 4), leading to a change in the relative absorption cross sections and a shift in the branching ratio curve to higher wavelengths (Fig. 5).

Observed changes in the branching ratio with application of the IR field are in reasonable qualitative agreement with theoretical calculations for five of the six excitation wavelengths. The smallest changes are predicted for the least sloped regions of the branching ratio curve, which occur at the central peak and edges of the absorption range. This is consistent with the experimental observation of no significant change to the branching ratios at 243 nm and 278 nm. Conversely, the most substantial changes in the branching ratio are expected for the most sloped regions of the curve – experimentally, this corresponds to excitation wavelengths of 213 nm, 216 nm, 230 nm, and 265 nm. Because application of the strong, nonresonant field led to a red-shifting of the branching ratio curve, theory and experiment agreed to a decrease in the branching ratio at 213 nm and 216 nm, and an increase in that ratio at 265 nm. The branching ratio increase that is observed experimentally at 265 nm is notably larger than the theory predicts for shift 2 and smaller than it predicts for shift 5, indicating that actual polarizabilities of the excited states may lie somewhere between the values used for the calculations of shifts 2 and 5.

The branching ratio at 230 nm increased considerably with application of the IR field. The relative enhancement of the slow channel at this photon energy disagrees with our theory and is quite striking compared to the behavior at other wavelengths; however, the observation is not necessarily unexpected. Experimental results at other wavelengths can be understood in terms of a change in the relative probabilities for dissociation through two adiabatic product channels. These observations are qualitatively corroborated by our theoretical model, which adequately describes how the cross-sections for excitation to and dissociation from a single electronic state (i.e., adiabatic transitions) are changed in the presence of a strong field. However, although previous studies report a predominately adiabatic picture of DI's dissociation dynamics, they also suggest a 7% contribution of nonadiabatic channels to the I^* product in the range of excitation wavelengths from 227-278 nm.[15, 29] The argument in these studies for the major possible source of nonadiabatic behavior is coupling between $^1\Pi_1$ and $^3\Pi_{0^+}$ in the Franck-Condon region. After an initial perpendicular excitation to the $^1\Pi_1$ state, the HI/DI molecule dissociates on the $^3\Pi_{0^+}$ state, forming the I* product.

We propose that, by changing the position of the avoided crossing between $^3\Pi_{0^+}$ and $^1\Pi_1$, the strong field influenced the nonadiabatic dynamics and contributed to the increase in the I* product channel which was observed at 230-nm excitation. Previous experimental observations support this hypothesis. In the ultrafast study of photon-catalyzed IBr photodissociation, Albert Stolow and coworkers[1, 2] observed the greatest influence of the strong nonresonant field (i.e., the maximum change in the branching ratio) when the nonresonant pulse arrived as the wavepacket traversed a crossing. A 30% increase in Br* production resulted at this intersection. If the crossing in DI was induced near 230-nm excitation by the strong electric field, a sensitive response to the excitation energy around the crossing is expected: for excitation above or below the crossing, the molecule's hopping probability is not measurably affected, and nonadiabaticity does not play a large role in the dissociation dynamics. These dynamics could not be accurately modeled by our level of theory. How the location of the crossings and coupling strengths vary as a function of the applied field is an interesting issue that clearly warrants more theoretical studies, but is beyond the scope of the present work.

Figure 6 presents a comparison of the theoretical branching ratio curves for each of the three electric field strengths used in our experiments: 5.1×10^7 V/cm, 5.8×10^7 V/cm, and 6.3×10^7 V/cm. Scaling factors for shift 2 were used for the results presented here. Consistent with experimental measurements, these calculations suggest no significant changes to the branching ratios with an increase of field strength of this magnitude.

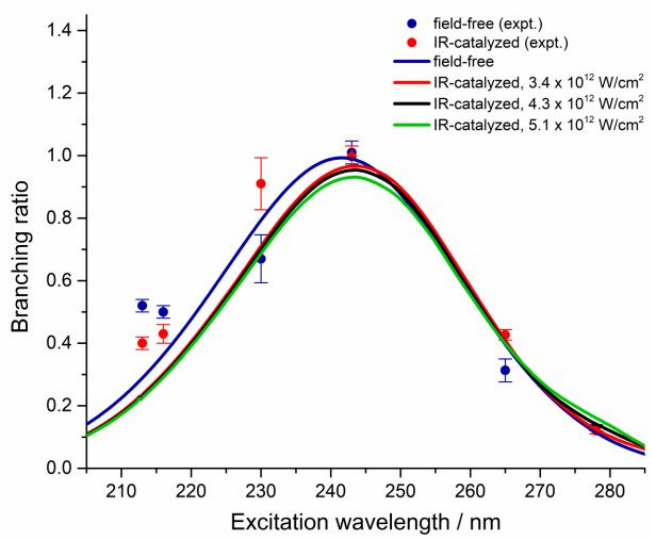

Fig. 6 Theoretically calculated branching ratio curves for the dissociation of DI under field-free conditions (black) and in the presence of a nonresonant IR field at 5.1×10^7 V/cm (red, 3.4×10^{12} W/cm^2), 5.8×10^7 V/cm (blue, 4.3×10^{12} W/cm^2), and 6.3×10^7 V/cm (green, 5.1×10^{12} W/cm^2). Error bars denote one standard deviation over 3-5 experimental data sets.

IV. Conclusions

In this study, DI was photodissociated at six excitation wavelengths between 213 – 278 nm in the presence of a nonresonant IR field (1064 nm). The use of nanosecond pulses allowed for determination of the average effect of the strong, nonresonant radiation on overall reaction yield. Changes in the measured branching ratios between field-free and strong field conditions confirm significant differences in dissociation dynamics. Because IR photons enhanced select dissociative pathways relative to others and were not consumed during the reaction, they behaved as catalysts in this process. Experiments and theoretical calculations confirmed that the mechanism for photon catalysis under these conditions was dynamic Stark shifting of potential energy surfaces rather than electric-field-induced alignment of reagent molecules.

Both the magnitude and direction of change in the branching ratios were dependent upon the excitation energy: branching ratios decreased at 213 and 216 nm by 23% and 14%, respectively, increased at 230 and 265 nm by 36% and 39%, and did not change significantly at 243 and 278 nm. Theoretical calculations predict a lowering in energy of excited state potentials, leading to a change in the relative absorption cross sections and a shift in the branching ratio curve toward higher wavelengths. Experiment and theory are in fair qualitative agreement for each excitation wavelength, with the exception of 230 nm. We suggest that the IR field increases nonadiabatic behavior at this photon energy that is not modelled by the level of theory employed, and further investigation is required.

Small changes in the magnitude of the IR field, between 5.1×10^7 V/cm and 6.3×10^7 V/cm, did not lead to observable changes in dissociation dynamics. Theory provided confirmation that the relative contributions of the two different channels was much more dependent upon the polarizabilities of the excited states than on small changes in the electric field strength. Future experiments could be completed at significantly higher electric field strengths to characterize the electric field strength dependence on the dynamics of this photon-catalyzed process. Nevertheless, the present study provides clear evidence of the effects of photon catalysis on the photodissociation dynamics of DI.

The dynamic Stark shift impacts all polarizable molecules, suggesting broad chemical applicability. Extension of photon catalysis studies to include bimolecular reactions, reactions involving polyatomic molecules, and reactions in condensed phases may build understanding of its potential for applicability beyond fundamental scientific research.

References

1. B. J. Sussman, D. Townsend, M. Y. Ivanov and A. Stolow, *Science*, 2006, **314**, 278-281.
2. A. Stolow, *Nature chemistry*, 2014, **6**, 759-760.
3. S. D. Fried, S. Bagchi and S. G. Boxer, *Science*, 2014, **346**, 1510.
4. M. Corrales, J. González-Vázquez, G. Balerdi, I. Solá, R. De Nalda and L. Bañares, *Nature chemistry*, 2014, **6**, 785-790.
5. J. González-Vázquez, I. R. Sola, J. Santamaria and V. S. Malinovsky, *The Journal of Physical Chemistry A*, 2007, **111**, 2670-2678.
6. B. Friedrich and D. Herschbach, *Physical Review Letters*, 1995, **74**, 4623.
7. A. Brown, *The Journal of chemical physics*, 2005, **122**, 084301.
8. D. N. Jodoin and A. Brown, *The Journal of chemical physics*, 2005, **123**, 054301.
9. N. Balakrishnan, A. Alekseyev and R. Buenker, *Chemical physics letters*, 2001, **341**, 594-600.
10. I. Levy and M. Shapiro, *The Journal of chemical physics*, 1988, **89**, 2900-2908.
11. G. Péoux, M. Monnerville, T. Duhoo and B. Pouilly, *The Journal of chemical physics*, 1997, **107**, 70-82.
12. A. G. Smolin, O. S. Vasyutinskii, G. G. Balint-Kurti and A. Brown, *The Journal of Physical Chemistry A*, 2006, **110**, 5371-5378.
13. D. Zhang, *Journal of mathematical chemistry*, 2010, **47**, 29-40.
14. M. H. Alexander, B. Pouilly and T. Duhoo, *The Journal of chemical physics*, 1993, **99**, 1752-1764.
15. S. R. Langford, P. M. Regan, A. J. Orr-Ewing and M. N. Ashfold, *Chemical physics*, 1998, **231**, 245-260.
16. F. Wang, I.-C. Lu, K. Yuan, Y. Cheng, M. Wu, D. H. Parker and X. Yang, *Chemical Physics Letters*, 2007, **449**, 18-22.
17. P. M. Regan, S. R. Langford, A. J. Orr-Ewing and M. N. Ashfold, *The Journal of chemical physics*, 1999, **110**, 281-288.
18. R. D. Clear, S. J. Riley and K. R. Wilson, *The Journal of Chemical Physics*, 1975, **63**, 1340-1347.
19. B. Huebert and R. Martin, *The Journal of Physical Chemistry*, 1968, **72**, 3046-3048.
20. Z. Xu, B. Koplitz and C. Wittig, *J. Phys. Chem.,* 1988, **92,** 5518-5523.
21. Z. Xu, B. Koplitz and C. Wittig, *The Journal of chemical physics*, 1987, **87**, 1062-1069.
22. Y. Matsumi, K. Tonokura, M. Kawasaki and T. Ibuki, *The Journal of chemical physics*, 1990, **93**, 7981-7985.
23. T. Kinugawa and T. Arikawa, *The Journal of chemical physics*, 1992, **96**, 4801-4804.

24. J. J. Larsen, H. Sakai, C. Safvan, I. Wendt-Larsen and H. Stapelfeldt, *The Journal of chemical physics*, 1999, **111**, 7774-7781.
25. K. J. Franks, H. Li and W. Kong,*The Journal of Chemical Physics,* 1999, **110**, 11779 - 11788.
26. H. Sakai, S. Minemoto, H. Nanjo, H. Tanji and T. Suzuki, *Physical Review Letters*, 2003, **90**, 083001-083001 - 083001-083004.
27. S.-M. Wang, K.-J. Yuan, Y.-Y. Niu, Y.-C. Han and S.-L. Cong, *Physical Review A*, 2006, **74**, 043406.
28. G. Maroulis, *Chem. Phys. Lett.*, 2000, **318**, 181-189.
29. A. J. R. Heck and D. W. Chandler, *Annual Review of Physical Chemistry*, 1995, **46**, 335-372.
30. J. Zhang, J. Jankunas, N. C.-M. Bartlett, N. T. Goldberg and R. N. Zare, *The Journal of chemical physics*, 2010, **132**, 084301.
31. M. A. Buntine, D. P. Baldwin, R. N. Zare and D. W. Chandler, *The Journal of chemical physics*, 1991, **94**, 4672-4675.
32. K. Koszinowski, N. T. Goldberg, A. E. Pomerantz and R. N. Zare, *The Journal of chemical physics*, 2006, **125**, 133503.
33. M. Mérawa, D. Bégué and A. Dargelos, *The Journal of Physical Chemistry A*, 2003, **107**, 9628-9633.
34. J. P. Camden, H. A. Bechtel, D. J. Ankeny Brown, A. E. Pomerantz, R. N. Zare and R. J. Le Roy, *The Journal of Physical Chemistry A*, 2004, **108**, 7806-7813.
35. A. B. Alekseyev, H.-P. Liebermann, D. B. Kokh and R. J. Buenker, *The Journal of Chemical Physics*, 2000, **113**, 6174-6185.
36. A. B. Alekseyev, D. B. Kokh and R. J. Buenker, *The Journal of Physical Chemistry A*, 2005, **109**, 3094-3096.
37. J. A. Coxon and P. G. Hajigeorgiou, *J. Molecular Spectroscopy*, 1991, **150**, 1-27.
38. M. D. Feit and J. A. Fleck, *The Journal of Chemical Physics*, 1983, **78**, 301-308.
39. N. Balakrishnan, C. Kalyanaraman and N. Sathyamurthy, *Phys. Rep.*, 1997, **280**, 79-144.
40. B. Friedrich, personal communication.

Conflicts to declare

There are no conflicts to declare.

Acknowledgements

This material is based upon work supported by the National Science Foundation under Grant No. 1464640 and Grant No. 1806334. K.H., J.M., and M.S. are grateful to Dr. Bretislav Friedrich, Fritz-Haber Institute, Berlin, Germany for useful discussions. N.B. is grateful to Keith Lawler for his assistance with computations of excited state polarizabilities of HI presented in the supplementary material.

Photon catalysis of deuterium iodide photodissociation

Kallie I. Hilsabeck [†a], Jana L. Meiser [†a], Mahima Sneha [†a], N. Balakrishnan[b], Richard N. Zare[a*]

[a] Department of Chemistry, Stanford University,
Stanford, CA, 94305, USA
[b] Department of Chemistry and Biochemistry, University of Nevada, Las Vegas,
Las Vegas, NV, 89154, USA

[†] These authors contributed equally to this research.

All correspondence should be addressed to rnz@stanford.edu.

A catalyst enhances a reaction pathway without itself being consumed or changed. Recently, there has been growing interest in the concept of "photon catalysis" in which nonresonant photons, which are neither absorbed nor scattered, promote reactions. The driving force behind this effect is the interaction between the strong electric field associated with a pulsed, focused laser and the polarizability of the reacting system. In this study, the effect of near-infrared, nonresonant radiation on the photodissociation of deuterium iodide is demonstrated. We use nanosecond pulses rather than time-resolved spectroscopy to investigate the average effect of the electric field on the branching ratio for forming D + I($^2P_{3/2}$) and D + I($^2P_{1/2}$). Changes in the measured D-atom speeds between field-free and strong-field conditions confirm substantial differences in dissociation dynamics. Both the magnitude and direction of change in the branching ratios are dependent upon the photodissociation wavelength. Experiments and theoretical calculations confirm that the mechanism for photon catalysis under these conditions is dynamic Stark shifting of potential energy surfaces rather than electric-field-induced alignment of reagent molecules.

I. Introduction

Chemists strive to achieve control over chemical reactions by manipulating such physical variables as pressure, temperature, solvent polarity, and reagent concentration; however, even thermodynamically favored reactions often resist yielding appreciable amounts of product because the kinetics are too slow. The key to unlocking such reactions is to find a suitable catalyst, a species that enhances the rate of a reaction without itself being used up or changed.

Catalysis is a vast and quickly developing area in chemical research with applications in several fields of science and technology. Standard examples of chemical catalysts include enzymes, organometallic complexes, and metal surfaces. Although very different in structure, each of these substances share a common function: through electric fields, they interface with specific bonds or functional groups within a reacting compound.[1, 2] The result of this action is to lower the energy of the transition state for a specific reaction pathway relative to others, thus enhancing its reaction rate. Applying electric forces[3] to reacting molecular systems can be achieved even in the absence of a traditional chemical catalyst, for example, through the application of a focused laser pulse.

Light exists as a propagating wave of electric and magnetic fields. For decades, the interaction of light with matter has been used to induce spectroscopic transitions through the resonant excitation of molecules to rotational, vibrational, and electronic excited states. The effect of nonresonant radiation is often considered to be insignificant and disregarded; however, this assumption is only valid in the limit of a "weak" field.[2] With pulsed lasers, it is possible to achieve electric field strengths that exceed by orders of magnitude the static field strengths supplied by common high-voltage power supplies. For

example, an IR laser pulse (1064 nm) of 4 W focused to a beam waist radius of 30 μm and having a duration of 10-11 ns, has a peak intensity of 3.4×10^{12} W/cm^2 and electric field strength, ε_0, on the order of 5.0×10^7 V/cm. At these high laser powers, nonresonant radiation, through its electric field, can influence the course of a reaction by interacting with the molecular system's polarizability α to lower an activation barrier directly. Because there is no net consumption of photons in this process, the photons behave as catalysts rather than reactants in a process referred to as photon catalysis, or laser field catalysis as it was first defined by Stolow and coworkers.[1, 2, 4, 5]

To elaborate, consider a simple collinear molecular system, e.g., the photodissociation of a linear molecule. For frequencies much greater than the reciprocal of the laser pulse duration, the Hamiltonian can be written in the following way:

$$\bar{\mathrm{H}} = H_0 + BJ^2 - \frac{1}{4}\varepsilon_0^2\left[\alpha_\perp + (\alpha_\parallel - \alpha_\perp)\cos^2\theta\right], \quad (1)$$

where $H_0 + BJ^2$ describes a rotating molecular system in the absence of an external field, ε_0 is the electric field strength, θ is the angle between the electric field and the molecular axis, and $\alpha_\parallel$ and $\alpha_\perp$ represent the polarizabilities of the linear system, parallel and perpendicular to the molecular axis.[6] Please note that possible interaction with a permanent dipole moment averages to zero and therefore is not included. The term in square brackets in this equation clearly outlines two possible effects of a strong, nonresonant electric field on a molecular system:

1) *Stark shift of energy levels* - The bracketed terms that are independent of θ result in a Stark shift of the molecule's potential energy surfaces. The distortion of these surfaces may alter adiabatic and/or nonadiabatic dissociation dynamics by impacting the intersection geometry and Landau-Zener hopping probabilities, thereby enhancing or depleting the contribution from the available channels to the total product yield.
2) *Alignment* - The term involving $\cos^2\theta$ mixes rotational levels, causing the molecular system to become aligned in the presence of a strong electric field. This behavior is most prevalent for atoms/molecules in the ground rotational state. The effect of alignment on the dissociation dynamics is dependent upon the anisotropy of the dissociation and the polarization of the strong electric field.

Hydrogen halide and dihalide molecules provide model theoretical[7-14] and experimental[15-23] systems for photodissociation reactions involving an excitation from the ground state to an electronically excited potential energy surface. Because they are well-characterized in the literature and exhibit significant polarizability even in the ground state, these simple molecules are also excellent starting points for the experimental demonstration of photon catalysis. To date, the most well-known observation of photon catalysis involved the photodissociation dynamics of IBr, a dihalide molecule. Stolow and coworkers[1] used time-resolved, ultrafast spectroscopy to confirm that application of a strong, nonresonant infrared (IR) field (λ = 800 nm) led to substantial changes in the relative contributions of two competing IBr dissociation channels. This study demonstrated one of the possible effects of strong, nonresonant radiation on a molecular system: dynamic Stark shifting of potential energy surfaces to energetically favor the formation of one product over another. For this system, with nearly purely repulsive excited state surfaces, the nonresonant field did not catalyze the reaction by lowering an energy barrier along any one excited potential surface. Instead, the IR field catalyzed one reaction pathway by enhancing its rate relative to another, without being consumed, through Stark shifting of potential energy surfaces. Another study by Bañares and coworkers[4] demonstrated that the presence of an ultrafast strong laser field gives rise to light induced conical intersections in the CH_3I

potentials, leading to a substantial change in the branching ratio of different product channels in the photolysis of this molecule.

It has also been experimentally observed that a second effect, alignment of reagent molecules by a nonresonant laser field, can lead to a change in the contribution of different channels to the overall product yield. Stapelfeldt *et al.*[24] demonstrated control over the ratio between two photodissociation channels of iodine (I_2) through application of a strong, near-IR laser pulse polarized either parallel or perpendicular to the polarization axis of the excitation laser pulse. This result is consistent with the anisotropic nature of the photodissociation: the two major product channels are related adiabatically to two different excited potential energy surfaces that are accessed through either a parallel or perpendicular transition, respectively. Therefore, one of the product channels is favored when the aligning and dissociating laser pulses are polarized in the same direction, and the other channel is favored when the two lasers are polarized perpendicularly to each other. Similar studies involving linear molecules like OCS (Sakai *et al.*[25]), as well as more complex compounds like pyrimidine (Franks *et al.* [26]), also have shown that it is possible to control a molecule's alignment using a strong electric field.

In the work presented here, we studied the impact of the two aforementioned effects of a strong, nonresonant, near-IR field on photodissociation of deuterium iodide (DI). As in the case of IBr, DI exhibits prompt dissociation from nearly purely repulsive surfaces. Two channels arise from the spin-orbit interactions in the iodine atom.[7-10, 15-20] The spin-orbit excited state of the I atom ($^2P_{1/2}$) is higher in energy than the ground state I atom ($^2P_{3/2}$) by 0.94 eV. Therefore, the dissociation channel D + I($^2P_{3/2}$), where the I is in its ground state, has higher kinetic energy disposed in the corresponding D atom and is known as the fast channel. The slow channel corresponds to the spin-orbit excited state of iodine, I($^2P/_{1/2}$), which hereafter will be denoted by I^*. By the necessity that total energy be conserved, this channel has slower-moving D atoms. The extent to which each channel is populated depends upon the potential energy curve to which the molecule is initially excited (i.e., the energy of the exciting photon), and the probability for nonadiabatic transitions within the Franck-Condon region (Fig. 1). The ratio of the respective reaction cross sections, σ, of the slow channel to the fast channel is referred to as the branching ratio, $\sigma[I^*]/\sigma[I]$. The wavelength dependence of the branching ratio in the absence of a strong electric field has previously been characterized, and is observed to peak approximately at 250 nm.[15] By monitoring changes in the branching ratio with application of strong, nonresonant radiation, experimental results provided insight into the photon-catalyzed process.

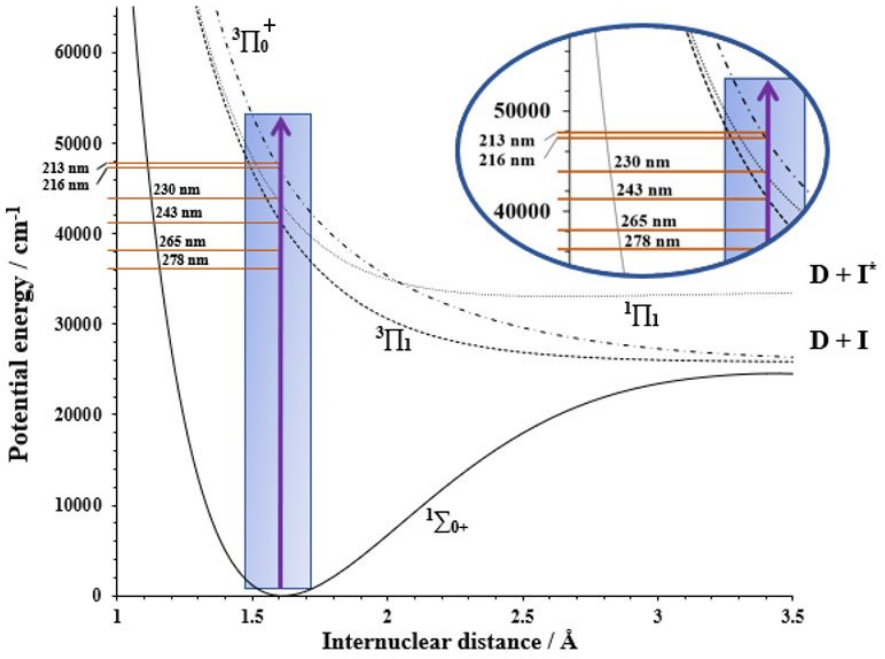

Fig. 1 Potential energy curves for the ground and low-lying excited electronic states of DI involved in one-photon dissociation. The parts of the potential that were sampled at each experimental excitation wavelength, within the Franck-Condon region, are illustrated schematically.

Simple theoretical calculations that model the effect of dynamic Stark shifting on the branching ratio were performed to complement and qualitatively support experimental results. The photodissociation dynamics were treated using the time-dependent wave packet formalism. Details of the field-free dynamics are given in prior works.[7-9] Although the photodissociation dynamics of HI in the presence of two-color, intense laser pulses has been reported previously,[27] the effect of a pulsed, nonresonant electric field on the dissociation dynamics and the I*/I branching ratio has not been theoretically explored. Below, we provide a brief description of the theoretical approach, following the methods given in Refs. 9 and 27.

The time-dependent Schrödinger equation was solved to describe the photodissociation dynamics of DI in the A band. Five electronic states were considered in the study: $X^1\Sigma^+$, $^3\Pi_1$, $^1\Pi_1$, $^3\Pi_{0^+}$, and $t^3\Sigma_1^+$, denoted $V_i(R)$, i = 1-5. The Schrödinger equation may be written as

$$i\hbar\frac{\partial\boldsymbol{\Psi}(R,t)}{\partial t} = \left[-\frac{\hbar^2}{2m}\boldsymbol{I}\frac{d^2}{dR^2} + \boldsymbol{U}(R)\right]\boldsymbol{\Psi}(R,t), \quad (2)$$

where $\boldsymbol{\Psi}$ is a column vector of wave functions with components ψ_i, $i = 1-5$, for the five electronic states, $\boldsymbol{I}$ is a 5×5 identity matrix, and $\boldsymbol{U}(R)$ is a 5×5 potential energy matrix with the diagonal elements,

$$U_i(R) = V_i(R) - \frac{1}{4}\alpha_i(R)\varepsilon_0(t)^2. \quad (3)$$

The second term of Eq. (3) denotes the Stark-shift of the potential curves due to the electric field. Rotational effects were ignored in our calculations, and the polarizability term was approximated by its

parallel component, with values taken from Maroulis[28] for the $X^1\Sigma^+$ state. The anisotropy of the polarizability is quite small for the ground state of HI, $\Delta\alpha = \alpha_{\parallel} - \alpha_{\perp} = 2.94$ au, compared to the parallel component, $\alpha_{\parallel} = 37.98$ au, at the equilibrium internuclear separation. The Stark shift was applied only to the excited state potential curves ($V_i(R)$, i = 2-5).

Alignment, the second possible effect of a nonresonant field, is also investigated experimentally. The studies on HI photodissociation by Langford *et al.*[15], and DI dissociation by Heck and Chandler[29] show that independent of wavelength of excitation, the fast and slow channels for both HI and DI result predominantly from adiabatic perpendicular and parallel transitions, respectively. Therefore, changing the relative polarizations of the near-IR pulse and exciting pulses allows for the deconvolution of the effects of Stark shifting and alignment on reaction outcome. This study is further distinguished from previous work because nanosecond pulses are employed to supply the field, which are much longer than the timescale of the reaction. This presents an opportunity to determine the more general effect that a nonresonant electric field had on modifying total reaction yield, rather than doing a time-resolved study. It is also more conducive to future extension of the effect beyond unimolecular reactions, e.g., to bimolecular reactions such as DI + D $\longrightarrow$ D_2 (v', j') + I.[30, 31]

II. Methods

Experimental Details

A detailed description of the experimental setup has been provided in previous publications.[32] For this set of experiments, a mixture of 5% DI (D 98%, Cambridge Isotopes Laboratories, Inc.) in an inert carrier gas (Ar, He) was expanded supersonically into a vacuum chamber through a pulsed valve (General Valve, Series 9) at a stagnation pressure of 10-15 psi. We observed no significant differences in the branching ratios using different carrier gases. The molecular beam was collimated through a 2 mm skimmer and intersected orthogonally by focused photolysis and photoionization (probe) lasers, as well as the IR laser (1064 nm) that supplied the strong electric field. Resulting positively charged D^+ ions were accelerated through a Wiley-McLaren time-of-flight (TOF) mass spectrometer and collected on a position-sensitive delay-line detector. Time and position information were used to extract lab-frame speed distributions for the product D^+ ions. The branching ratios were calculated by integrating the relative areas under the slow and fast channel peaks in the speed distributions.

DI photodissociation was carried out at six wavelengths in the A-band between 213 and 278 nm, both with and without the strong electric field supplied by the near-IR laser. Under each set of conditions, three to five reproducible data sets, averaging over 3000-4000 ions, were collected. For each experiment, the photolysis laser power was maintained at approximately 10-20 μJ. The D-atom product was ionized using (2+1) resonance enhanced multiphoton ionization (REMPI) via the 2s – 1s transition at approximately 243 nm. Under the application of the strong electric field, the REMPI line was red-shifted 10 - 20 pm to account for the observed Stark shift of the D-atom signal. A probe laser power of 5 μJ was sufficient for this experimental setup. The average power peak intensity of the IR laser was maintained between 3.4×10^{12} W/cm^2 and 5.1×10^{12} W/cm^2, which, when focused with a lens of f = 35 cm, corresponds to an electric field strength of approximately 5.1×10^7 V/cm to 6.3×10^7 V/cm in the interaction volume. Low powers of the UV lasers ensured that the strong electric field was solely produced by the IR laser. A detailed description of the method of background subtraction is provided in the supplementary information (Fig. S1).

Two techniques were used for D-atom detection. For excitation wavelengths of 213 nm, 216 nm, 243 nm, and 278 nm, the Doppler-free technique was implemented. Two counterpropagating UV lasers were overlapped spatially and temporally, and their wavelengths were chosen such that

combined they achieved resonance with the (2+1)-REMPI line at 243 nm. The dissociation laser was set at higher power so that it solely photolyzed the DI molecule. Minimal photolysis contamination from the other UV laser was subtracted as background. Because both lasers contributed to the probe step and were traveling in opposite directions toward the interaction region, D atoms were ionized regardless of their speed with respect to the laser propagation direction. This condition strongly increased the signal without impacting the amount of background in our experiments. Furthermore, as the Doppler-free technique removed the requirement to perform a scan over the Doppler range, it reduced inconsistencies arising from power and overlap fluctuations of the lasers throughout data collection and produced speed distributions with a more Gaussian shape.

For 265 nm and 230 nm excitation, a traditional pump-probe setup was used. DI molecules were first dissociated by the pump laser and, after a short time delay of 3 ns, the resulting D-atom product was ionized using (2+1)-REMPI via the 2s – 1s transition at approximately 243 nm. The probe laser wavelength was scanned over the Doppler range. This detection technique was chosen for these two wavelengths because the complementary UV wavelength required to fulfill the Doppler-free condition either produced strongly overlapping peaks in the speed distribution (265 nm, Fig.S2) or caused an overwhelming amount of multiphoton background with the IR (230 nm).

The ultraviolet laser light of appropriate wavelengths for the photolysis and photoionization processes was attained in two ways: frequency tripling the output of a dye laser (Lambda Physik, LPD 3000) pumped by the second harmonic of an Nd:YAG^{3+} laser (Spectra Physics, GCR Series), or frequency doubling the output of a dye laser (Lambda Physik, LPD 3000) pumped by the third harmonic of an Nd:YAG^{3+} laser (Quanta-Ray, DCR-3). The strong electric field was supplied by the fundamental of a third Nd:YAG^{3+} laser (Spectra Physics, GCR Series) at 1064 nm. All frequency mixing was achieved using BBO crystals.

Computational Details

Theoretical calculations correspond to a pulse width of τ = 500 fs. Although we used a much longer IR pulse for our experiments, the probability for excitation and dissociation from each excited potential surface reached a steady state within about 50 fs, by which time the electric field also had reached 97% of its peak value (Fig. S3). Therefore, this approximation is reasonable for comparison with our experimental results.

In the absence of any literature results on the polarizabilities of HI for the various excited electronic states considered here, we have approximated the excited state polarizabilities, α_i(R)= α_1(R)×*f(i), i* = 2-5, where α_1(R) is the polarizability of the ground state and *f(i), i* = 2-5 are scaling factors for the excited state polarizabilities. We have taken wide latitude in choosing the scaling factors to explore any unusually large effect induced by the electric field. Different sets of calculations were performed with different values of the scaling parameters to examine the sensitivity of results to the shift in the excited state potentials induced by the electric field. Five different sets of calculations were performed for a given laser intensity with the excited state polarizabilities varied by a factor of 1.2 to a factor of 15. They are listed below as Shift 1 through Shift 5:

Shift1: $f(2) = 1.2, f(3) = 1.3, f(4) = 1.5, f(5) = 1.5$
Shift2: $f(2) = 2.0, f(3) = 2.5, f(4) = 3.0, f(5) = 3.0$
Shift3: $f(2) = 3.0, f(3) = 3.5, f(4) = 4.0, f(5) = 4.0$
Shift4: $f(2) = 4.0, f(3) = 4.5, f(4) = 5.0, f(5) = 5.0$
Shift5: $f(2) = 10.0, f(3) = 11.0, f(4) = 15.0, f(5) = 15.0$

In each case, $f(4)$ and $f(5)$ were assumed to be the same, as excited state 5 does not contribute appreciably to the one-photon dissociation process in the wavelength range reported here. Although

this choice of scaling factors is rather arbitrary, large variations in excited state polarizabilities with factors from 2-6 have been reported for diatomic molecules such as LiH and NaH.[33] Preliminary ab initio calculations without the inclusion of spin-orbit coupling also suggest a factor of 2 or higher values for the excited state polarizabilities with strong anisotropic components. Table S1 presents details of this calculation in the supplementary information.

The off-diagonal elements $U_{1i}(R) = U_{i1}(R)$, i = 2-5 of $\boldsymbol{U}(R)$ denote the field-induced couplings, which in the dipole approximation are given by $U_{1i}(R) = -\mu_{1,i}(R)\varepsilon_0(t)\cos(\omega t)$, i = 2-5 where $\mu_{1,i}(R)$ are the R-dependent transition dipole moments between the ground state and the excited electronic states, i = 2-5. The electric field is defined as $\varepsilon_0(t) = \varepsilon_0 g(t)$, where ε_0 is the peak field strength, and the envelope function g(t) is taken to be a Gaussian centered at t = 0, $g(t) = \exp[-4\ln(2)t^2/\tau^2]$ with full-width τ at half-maximum.

The excited-state potential curves and transition dipole moments are taken from Camden *et al.*,[34] which provide experimentally calibrated parameters. We used parameters corresponding to model 1 in Table 3 of Camden *et al.*[34] The branching ratio is very sensitive to the slope of the excited state potential curves in the Franck-Condon region, and the potential curves and dipole moment functions of model 1 yield better agreement with experiment than the ab initio potential curves and transition dipole moments of Alekseyev *et al.*[35] However, Alekseyev *et al.*[36] have also argued that a slight upward shift of approximately 500 cm^{-1} of the ab initio computed excited triplet potential curves and a 5% increase in the $(^1\Pi_1, ^3\Pi_1)\leftarrow X$ transition dipole moments yield results in close agreement with experiment, an analysis that also favors model 1 parameters. For the ground $X^1\Sigma^+$ state, we used the potential energy curve of Coxon and Hajigeorgiou[37] in the short-range and merged it smoothly with the ab initio potential of Alekseyev *et al.*[35] for R > 6.3 bohr. We have also included the spin-rotation coupling between the $^1\Pi_1$ and $^3\Pi_{0^+}$ states as an off-diagonal matrix element $U_{34}(R) = U_{43}(R)$, but this has a negligible effect on the branching ratio as found for field-free dynamics in Ref. 9. Although we have included the $t^3\Sigma_1^+$ electronic state correlating with I* channel in our calculations, its effect is not important and it does not contribute to I* channel at the excitation wavelengths considered in this work.

The Schrödinger equation was solved using the split-operator method[38] with appropriate absorbing boundary conditions.[39] The wave packet was initialized as $\psi_1(R,t=0) = \phi_{v=0,j=0}(R)$, $\psi_i(R,t=0) = 0, i = 2-5$, where $\phi_{v=0,j=0}(R)$ is the rovibrational ground state wave function of the $X^1\Sigma^+$ state. A radial grid of 512 points in the range R = 2-20 au was used to discretize the wave packet. See Ref. 9 for more details. Diagonalization of the potential matrix at each time step of the propagation yielded an adiabatic "light-induced" potential.

II. Results & Discussions

Deuterium iodide was photodissociated under field-free conditions and in the presence of the strong electric AC field supplied by a nonresonant, near-IR laser pulse at 1064 nm. Figures 2a-2f present the measured D-atom speed distributions for six excitation wavelengths spanning the A band: Fig. 2a at 213 nm, Fig. 2b at 216 nm, Fig. 2c at 230 nm, Fig. 2d at 265 nm, Fig. 2e at 243 nm, and Fig. 2f at 278 nm. Table S2 lists the fast and slow D-atom speeds for the excitation wavelengths used in this study. For these sets of experiments, the excitation laser pulse was polarized vertically, and the IR laser pulse was polarized horizontally.

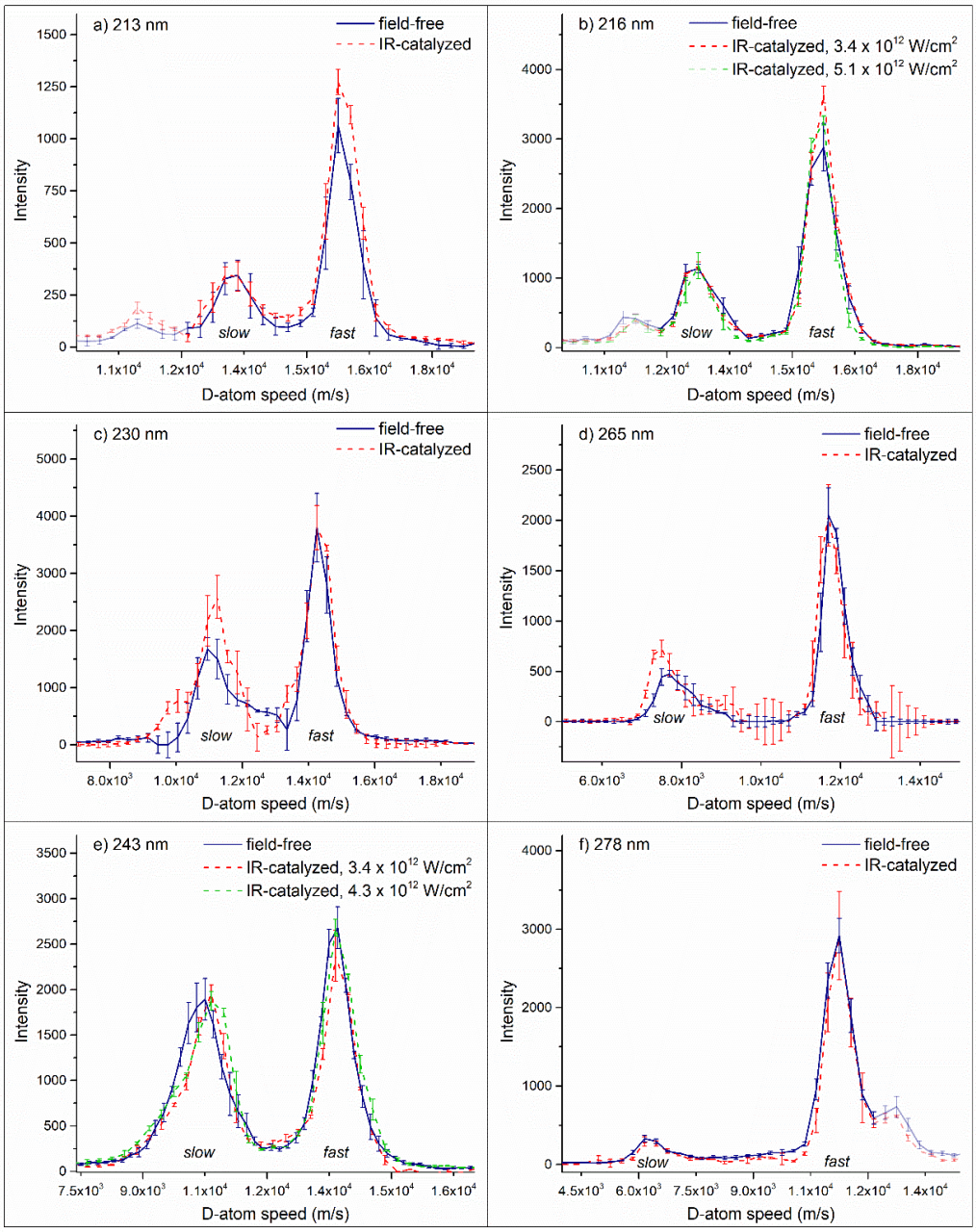
a) 213 nm
field-free
IR-catalyzed
b) 216 nm
field-free
IR-catalyzed, 3.4 x 10^12 W/cm^2
IR-catalyzed, 5.1 x 10^12 W/cm^2
c) 230 nm
field-free
IR-catalyzed
d) 265 nm
field-free
IR-catalyzed
e) 243 nm
field-free
IR-catalyzed, 3.4 x 10^12 W/cm^2
IR-catalyzed, 4.3 x 10^12 W/cm^2
f) 278 nm
field-free
IR-catalyzed
Intensity
D-atom speed (m/s)
slow
fast

Fig. 2 D-atom speed distributions for the photodissociation of DI at a series of excitation wavelengths: a) 213 nm, b) 216 nm, c) 230 nm, d) 265 nm, e) 243 nm, and f) 278 nm. The blue lines represent data collected in the absence of a strong electric field (field-free), and the red dashed lines represent data collected at an IR peak intensity of 3.4×10^{12} W/cm^2 ($\varepsilon_0 = 5.1 \times 10^7$ V/cm, IR-catalyzed). The green dashed lines in b) and e) are for experiments performed at higher IR peak intensities of 4.3×10^{12} W/cm^2 and 5.1×10^{12} W/cm^2, respectively ($\varepsilon_0 = 5.8 \times 10^7$ V/cm, and 6.3×10^7 V/cm). Error bars denote one standard deviation over 3-5 experimental data sets. A third peak is observed in the case of Fig. 2a, 2b, and 2f, here marked in a lighter shade for clarity, which originates from photolysis by the complementary Doppler-free probe laser. The shoulders on the leading edges of the fast and slow channel peaks in Fig. 2c are also consistent with 243-nm dissociation by the probe laser.

The experimental branching ratios under field-free conditions were in reasonable agreement with previously published values.[15] Upon application of a strong AC field that encompassed the entire photodissociation process, we observed significant changes in the branching ratios to one standard deviation. These experimental findings provide clear evidence of the measurable effect of a nonresonant IR field on the photodissociation dynamics of DI. Furthermore, because IR photons were neither absorbed nor changed during this process, they acted as catalysts to selectively lower activation barriers for one pathway relative to another.

Both the magnitude and direction of this change were dependent upon the excitation energy. At 213 nm and 216 nm (Fig. 2a and 2b), the branching ratio decreased by 23% and 14%, respectively, under strong field conditions, suggesting that the *fast* product channel was enhanced relative to the slow channel by the application of the IR field in this wavelength range. Conversely, at 230 nm and 265 nm (Fig. 2c and 2d), the branching ratio increased significantly by 36% and 39%, respectively, which indicates a relative increase in the *slow* channel contribution with application of the IR field. No measurable change in the branching ratio was perceived for photodissociation at 243 nm or 278 nm (Fig. 2e and 2f). Higher intensity IR experiments were performed for excitation at 216 nm and 243 nm. As is evident from Fig. 2b and 2e, this increase in electric field strength was not sufficient to produce a measurable change from the branching ratio at the lower IR power. Table 1 summarizes the results.

Table 1 Experimentally measured branching ratios for the photodissociation of DI in the presence and absence of a strong, nonresonant IR field. Uncertainties represent one standard deviation over 3-5 experimental data sets.

Excitation Wavelength (nm)	IR Field-free Branching Ratio	Branching Ratio for IR Peak Intensity = 3.4×10^{12} W/cm^2 ($\varepsilon_0 = 5.1 \times 10^7$ V/cm)[a]
213	0.52 ±0.02	0.40 ±0.02
216	0.50 ±0.02	0.43 ±0.02
230	0.67 ±0.08	0.91 ±0.08
243	1.01 ±0.04	1.00 ±0.03
265	0.31 ±0.04	0.43 ±0.02
278 (H)[b]	0.13 ±0.01	0.12 ±0.01
278 (V)[b]	0.13 ±0.01	0.12±0.01

[a]For 243-nm and 216-nm excitation, IR experiments were also performed at $\varepsilon_0 = 5.8 \times 10^7$ V/cm and 6.3×10^7 V/cm, but there were no measurable changes from the branching ratio at 5.1×10^7 V/cm.
[b]For 278-nm excitation, data were collected with the IR laser polarized horizontally (H) and vertically (V).

A third peak was observed in the case of Fig. 2a, 2b and 2f. As mentioned previously, the Doppler-free probing technique used for these excitation wavelengths involved two counterpropagating lasers that can each contribute to photolysis. These additional peaks were the result of a small amount of DI photolysis by the other UV laser, which could not be fully accounted for in the background subtraction. However, as these peaks were well-separated from the slow and fast channels resulting from the excitation wavelength, they did not interfere with branching ratio determination. Similarly, small shoulders on the leading edges of the slow and fast channel peaks in Fig. 2c corresponded to 243-nm dissociation by the probe laser. Shoulders were not included in the area that was integrated for the branching ratio calculations; however, inclusion of the shoulder for both the slow and fast channel peaks did not cause the branching ratio to fall outside of the currently reported uncertainty because the branching ratio at 243 nm was approximately equal to 1 for both the field-free and IR-field cases.

It should also be noted that the two excitation wavelengths for which an increase in the slow channel were observed, 230 nm and 265 nm, were also the two wavelengths that employed the pump-probe approach. To confirm that this result was not caused by a systematic bias introduced by the detection technique, the experiments at 243-nm excitation were repeated using a one-laser, pump-probe approach. With both the Doppler-free and pump-probe techniques, the same result was observed: no change in branching ratio was detected with application of the strong field (Fig. S4a and S4b). Furthermore, the experiments at 230 nm were repeated with a 0 ns delay instead of 3 ns to ensure that the enhancement in the slow channel was not artificially created because of the faster moving atoms escaping the interaction volume before ionization. Measured speed distributions and branching ratios were not influenced by a time delay of this magnitude, under either field-free or IR-field conditions. Collectively, these results indicate that no systematic bias existed in our detection setup.

Degree of Alignment

Because the slow and fast channels correspond predominately to parallel and perpendicular transitions, respectively, alignment of reactant molecules with the electric field should favor one channel over the other, resulting in products with different branching ratios. In the experiments presented to this point, the excitation laser and IR laser were polarized perpendicularly to one another, and any significant alignment would have favored the formation of faster-moving D atoms. To evaluate the extent of alignment in the beam, we repeated the experiments at an excitation wavelength of 278 nm with a vertical polarization of the IR beam, parallel to the polarization of the excitation laser pulse (Fig. 3).

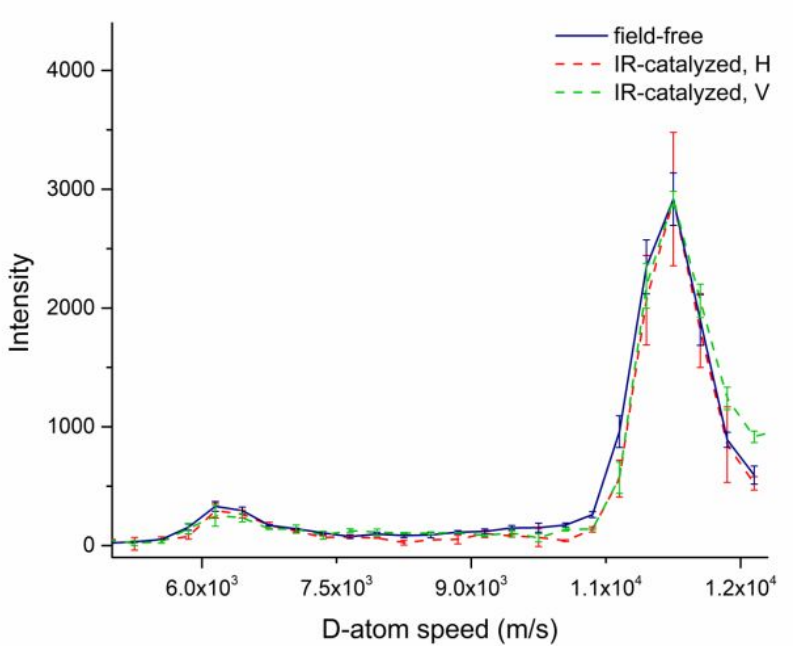

Fig. 3 D-atom speed distributions for the photodissociation of DI at 278 nm in the absence (blue line) and presence of vertically polarized (red dashed line) and horizontally polarized (green dashed line) IR field. Error bars denote one standard deviation over 3-5 experimental data sets.

As Fig. 3 and Table 1 indicate, the branching ratio in the presence of the strong field was independent of the polarization of the IR laser pulse relative to that of the excitation laser pulse at an excitation wavelength of 278 nm. Calculations predict that most of the alignment should occur for molecules in the ground rotational state, J = 0.[40] To determine the percentage of molecules present in the ground rotational state, the rotational distribution of DI in the molecular beam was measured. A large iodide ion background signal at the desired wavelengths precluded a quantitative measurement; however, qualitatively it was confirmed that there were roughly five times more molecules in the J = 1 level than in the J = 0 level, and that a discernable DI signal existed for rotational levels up to J = 10. Figure S5 in the SI displays an approximation for the rotational distribution of DI in our molecular beam. As the majority of the DI molecules in the molecular beam have non-zero rotational energy ($J \neq 0$), this result is consistent with no detectable alignment by an external electric field at an excitation wavelength of 278 nm (Fig. 3). This result is general, as alignment is not expected to be wavelength-dependent. The negligible impact of alignment under these experimental conditions suggests that the observed photon catalysis effect arose primarily because of the dynamic Stark shifting of potential energy surfaces, rather than electric-field-induced alignment.

Dynamic Stark-shifting of Potential Surfaces

Theoretical calculations were performed to make a qualitative prediction about how the dynamic Stark shifting of potential energy surfaces is expected to impact the relative contributions of the slow and fast channels to the dissociation of DI. Excited state polarizabilities were scaled up from the ground state over a range of scaling factors, as described above, to give an estimate of the expected Stark shifts. At an electric field strength of 5.1×10^7 V/cm, shifts 1-4, corresponding to different scaling factors, yielded comparable results. Conversely, shift 5 displayed an entirely different behavior that suggests that the scaled polarizabilities used were unrealistically large. This result is reflected in the

shifted potential energy curves and branching ratios presented in Fig. 4 and 5. In moving forward with the discussion, we take shift 2 as an acceptable approximation for the excited state polarizabilities.

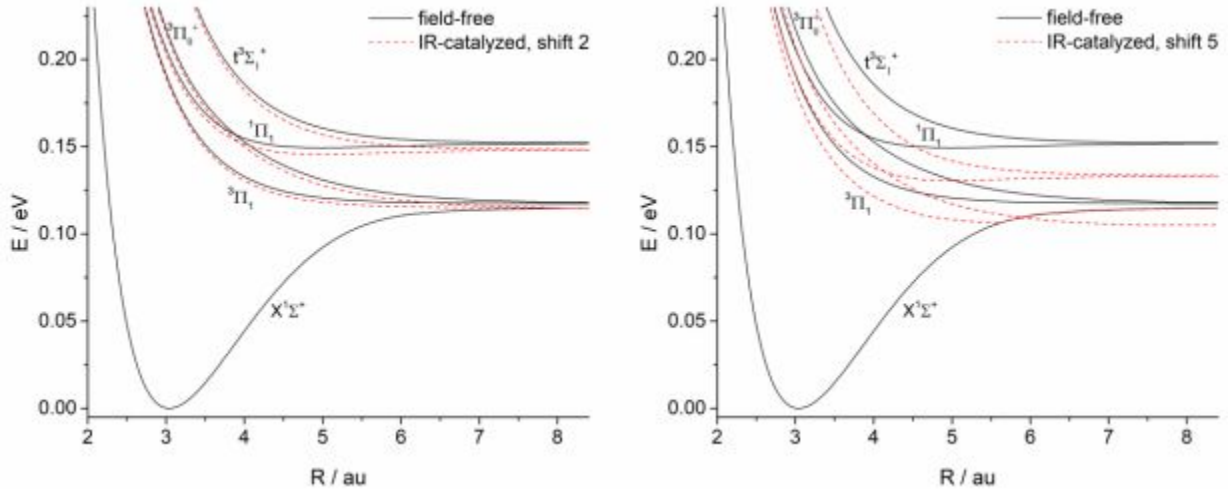

Fig. 4 Potential energy curves for the one-photon dissociation of DI under field-free (black, solid) and IR-catalyzed (red, dashed) conditions using the polarizabilities of a) shift 2 and b) shift 5. The electric field strength for these calculations was 5.1×10^7 V/cm.

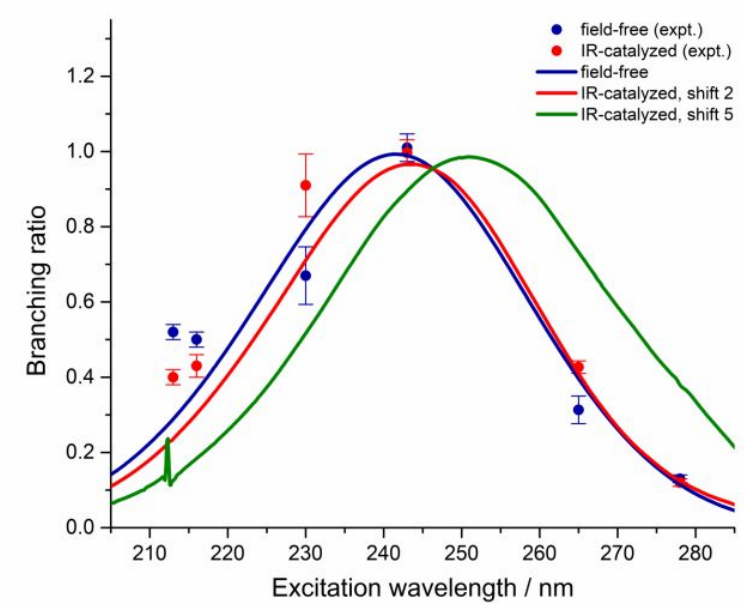

Fig. 5 Experimentally and theoretically determined branching ratios for the photolysis of DI, both in the presence (red and green) and absence (blue) of the strong IR field at 5.1×10^7 V/cm. Results of calculations for shifts 2 (red) and 5 (green) are displayed. Error bars denote one standard deviation over 3-5 experimental data sets.

Comparison of the experimental and theoretical data, presented in Fig. 5, clearly shows that the theory cannot quantitatively describe this system or the effect of the nonresonant IR field on its dynamics. However, theoretical calculations do provide qualitative insight into the photon-catalyzed

process. The predicted effect of the nonresonant field is to shift the excited potentials to lower energies (Fig. 4), leading to a change in the relative absorption cross sections and a shift in the branching ratio curve to higher wavelengths (Fig. 5).

Observed changes in the branching ratio with application of the IR field are in reasonable qualitative agreement with theoretical calculations for five of the six excitation wavelengths. The smallest changes are predicted for the least sloped regions of the branching ratio curve, which occur at the central peak and edges of the absorption range. This is consistent with the experimental observation of no significant change to the branching ratios at 243 nm and 278 nm. Conversely, the most substantial changes in the branching ratio are expected for the most sloped regions of the curve – experimentally, this corresponds to excitation wavelengths of 213 nm, 216 nm, 230 nm, and 265 nm. Because application of the strong, nonresonant field led to a red-shifting of the branching ratio curve, theory and experiment agreed to a decrease in the branching ratio at 213 nm and 216 nm, and an increase in that ratio at 265 nm. The branching ratio increase that is observed experimentally at 265 nm is notably larger than the theory predicts for shift 2 and smaller than it predicts for shift 5, indicating that actual polarizabilities of the excited states may lie somewhere between the values used for the calculations of shifts 2 and 5.

The branching ratio at 230 nm increased considerably with application of the IR field. The relative enhancement of the slow channel at this photon energy disagrees with our theory and is quite striking compared to the behavior at other wavelengths; however, the observation is not necessarily unexpected. Experimental results at other wavelengths can be understood in terms of a change in the relative probabilities for dissociation through two adiabatic product channels. These observations are qualitatively corroborated by our theoretical model, which adequately describes how the cross-sections for excitation to and dissociation from a single electronic state (i.e., adiabatic transitions) are changed in the presence of a strong field. However, although previous studies report a predominately adiabatic picture of DI's dissociation dynamics, they also suggest a 7% contribution of nonadiabatic channels to the I^* product in the range of excitation wavelengths from 227-278 nm.[15, 29] The argument in these studies for the major possible source of nonadiabatic behavior is coupling between $^1\Pi_1$ and $^3\Pi_{0^+}$ in the Franck-Condon region. After an initial perpendicular excitation to the $^1\Pi_1$ state, the HI/DI molecule dissociates on the $^3\Pi_{0^+}$ state, forming the I* product.

We propose that, by changing the position of the avoided crossing between $^3\Pi_{0^+}$ and $^1\Pi_1$, the strong field influenced the nonadiabatic dynamics and contributed to the increase in the I* product channel which was observed at 230-nm excitation. Previous experimental observations support this hypothesis. In the ultrafast study of photon-catalyzed IBr photodissociation, Albert Stolow and coworkers[1, 2] observed the greatest influence of the strong nonresonant field (i.e., the maximum change in the branching ratio) when the nonresonant pulse arrived as the wavepacket traversed a crossing. A 30% increase in Br* production resulted at this intersection. If the crossing in DI was induced near 230-nm excitation by the strong electric field, a sensitive response to the excitation energy around the crossing is expected: for excitation above or below the crossing, the molecule's hopping probability is not measurably affected, and nonadiabaticity does not play a large role in the dissociation dynamics. These dynamics could not be accurately modeled by our level of theory. How the location of the crossings and coupling strengths vary as a function of the applied field is an interesting issue that clearly warrants more theoretical studies, but is beyond the scope of the present work.

Figure 6 presents a comparison of the theoretical branching ratio curves for each of the three electric field strengths used in our experiments: 5.1×10^7 V/cm, 5.8×10^7 V/cm, and 6.3×10^7 V/cm. Scaling factors for shift 2 were used for the results presented here. Consistent with experimental measurements, these calculations suggest no significant changes to the branching ratios with an increase of field strength of this magnitude.

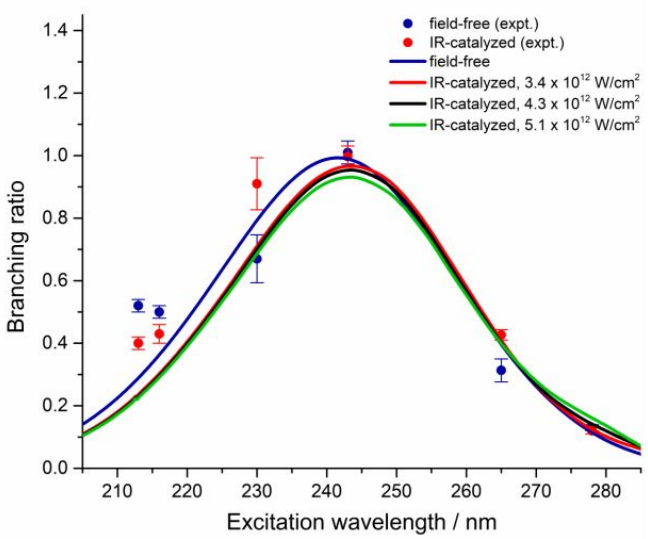

Fig. 6 Theoretically calculated branching ratio curves for the dissociation of DI under field-free conditions (black) and in the presence of a nonresonant IR field at 5.1×10^7 V/cm (red, 3.4×10^{12} W/cm^2), 5.8×10^7 V/cm (blue, 4.3×10^{12} W/cm^2), and 6.3×10^7 V/cm (green, 5.1×10^{12} W/cm^2). Error bars denote one standard deviation over 3-5 experimental data sets.

IV. Conclusions

In this study, DI was photodissociated at six excitation wavelengths between 213 – 278 nm in the presence of a nonresonant IR field (1064 nm). The use of nanosecond pulses allowed for determination of the average effect of the strong, nonresonant radiation on overall reaction yield. Changes in the measured branching ratios between field-free and strong field conditions confirm significant differences in dissociation dynamics. Because IR photons enhanced select dissociative pathways relative to others and were not consumed during the reaction, they behaved as catalysts in this process. Experiments and theoretical calculations confirmed that the mechanism for photon catalysis under these conditions was dynamic Stark shifting of potential energy surfaces rather than electric-field-induced alignment of reagent molecules.

Both the magnitude and direction of change in the branching ratios were dependent upon the excitation energy: branching ratios decreased at 213 and 216 nm by 23% and 14%, respectively, increased at 230 and 265 nm by 36% and 39%, and did not change significantly at 243 and 278 nm. Theoretical calculations predict a lowering in energy of excited state potentials, leading to a change in the relative absorption cross sections and a shift in the branching ratio curve toward higher wavelengths. Experiment and theory are in fair qualitative agreement for each excitation wavelength, with the exception of 230 nm. We suggest that the IR field increases nonadiabatic behavior at this photon energy that is not modelled by the level of theory employed, and further investigation is required.

Small changes in the magnitude of the IR field, between 5.1×10^7 V/cm and 6.3×10^7 V/cm, did not lead to observable changes in dissociation dynamics. Theory provided confirmation that the relative contributions of the two different channels was much more dependent upon the polarizabilities of the excited states than on small changes in the electric field strength. Future experiments could be completed at significantly higher electric field strengths to characterize the electric field strength dependence on the dynamics of this photon-catalyzed process. Nevertheless, the present study provides clear evidence of the effects of photon catalysis on the photodissociation dynamics of DI.

The dynamic Stark shift impacts all polarizable molecules, suggesting broad chemical applicability. Extension of photon catalysis studies to include bimolecular reactions, reactions involving polyatomic molecules, and reactions in condensed phases may build understanding of its potential for applicability beyond fundamental scientific research.

References

1. B. J. Sussman, D. Townsend, M. Y. Ivanov and A. Stolow, *Science*, 2006, **314**, 278-281.
2. A. Stolow, *Nature chemistry*, 2014, **6**, 759-760.
3. S. D. Fried, S. Bagchi and S. G. Boxer, *Science*, 2014, **346**, 1510.
4. M. Corrales, J. González-Vázquez, G. Balerdi, I. Solá, R. De Nalda and L. Bañares, *Nature chemistry*, 2014, **6**, 785-790.
5. J. González-Vázquez, I. R. Sola, J. Santamaria and V. S. Malinovsky, *The Journal of Physical Chemistry A*, 2007, **111**, 2670-2678.
6. B. Friedrich and D. Herschbach, *Physical Review Letters*, 1995, **74**, 4623.
7. A. Brown, *The Journal of chemical physics*, 2005, **122**, 084301.
8. D. N. Jodoin and A. Brown, *The Journal of chemical physics*, 2005, **123**, 054301.
9. N. Balakrishnan, A. Alekseyev and R. Buenker, *Chemical physics letters*, 2001, **341**, 594-600.
10. I. Levy and M. Shapiro, *The Journal of chemical physics*, 1988, **89**, 2900-2908.
11. G. Péoux, M. Monnerville, T. Duhoo and B. Pouilly, *The Journal of chemical physics*, 1997, **107**, 70-82.
12. A. G. Smolin, O. S. Vasyutinskii, G. G. Balint-Kurti and A. Brown, *The Journal of Physical Chemistry A*, 2006, **110**, 5371-5378.
13. D. Zhang, *Journal of mathematical chemistry*, 2010, **47**, 29-40.
14. M. H. Alexander, B. Pouilly and T. Duhoo, *The Journal of chemical physics*, 1993, **99**, 1752-1764.
15. S. R. Langford, P. M. Regan, A. J. Orr-Ewing and M. N. Ashfold, *Chemical physics*, 1998, **231**, 245-260.
16. F. Wang, I.-C. Lu, K. Yuan, Y. Cheng, M. Wu, D. H. Parker and X. Yang, *Chemical Physics Letters*, 2007, **449**, 18-22.
17. P. M. Regan, S. R. Langford, A. J. Orr-Ewing and M. N. Ashfold, *The Journal of chemical physics*, 1999, **110**, 281-288.
18. R. D. Clear, S. J. Riley and K. R. Wilson, *The Journal of Chemical Physics*, 1975, **63**, 1340-1347.
19. B. Huebert and R. Martin, *The Journal of Physical Chemistry*, 1968, **72**, 3046-3048.
20. Z. Xu, B. Koplitz and C. Wittig, *J. Phys. Chem.,* 1988, **92,** 5518-5523.
21. Z. Xu, B. Koplitz and C. Wittig, *The Journal of chemical physics*, 1987, **87**, 1062-1069.
22. Y. Matsumi, K. Tonokura, M. Kawasaki and T. Ibuki, *The Journal of chemical physics*, 1990, **93**, 7981-7985.
23. T. Kinugawa and T. Arikawa, *The Journal of chemical physics*, 1992, **96**, 4801-4804.

24. J. J. Larsen, H. Sakai, C. Safvan, I. Wendt-Larsen and H. Stapelfeldt, *The Journal of chemical physics*, 1999, **111**, 7774-7781.
25. K. J. Franks, H. Li and W. Kong,*The Journal of Chemical Physics,* 1999, **110**, 11779 - 11788.
26. H. Sakai, S. Minemoto, H. Nanjo, H. Tanji and T. Suzuki, *Physical Review Letters*, 2003, **90**, 083001-083001 - 083001-083004.
27. S.-M. Wang, K.-J. Yuan, Y.-Y. Niu, Y.-C. Han and S.-L. Cong, *Physical Review A*, 2006, **74**, 043406.
28. G. Maroulis, *Chem. Phys. Lett.*, 2000, **318**, 181-189.
29. A. J. R. Heck and D. W. Chandler, *Annual Review of Physical Chemistry*, 1995, **46**, 335-372.
30. J. Zhang, J. Jankunas, N. C.-M. Bartlett, N. T. Goldberg and R. N. Zare, *The Journal of chemical physics*, 2010, **132**, 084301.
31. M. A. Buntine, D. P. Baldwin, R. N. Zare and D. W. Chandler, *The Journal of chemical physics*, 1991, **94**, 4672-4675.
32. K. Koszinowski, N. T. Goldberg, A. E. Pomerantz and R. N. Zare, *The Journal of chemical physics*, 2006, **125**, 133503.
33. M. Mérawa, D. Bégué and A. Dargelos, *The Journal of Physical Chemistry A*, 2003, **107**, 9628-9633.
34. J. P. Camden, H. A. Bechtel, D. J. Ankeny Brown, A. E. Pomerantz, R. N. Zare and R. J. Le Roy, *The Journal of Physical Chemistry A*, 2004, **108**, 7806-7813.
35. A. B. Alekseyev, H.-P. Liebermann, D. B. Kokh and R. J. Buenker, *The Journal of Chemical Physics*, 2000, **113**, 6174-6185.
36. A. B. Alekseyev, D. B. Kokh and R. J. Buenker, *The Journal of Physical Chemistry A*, 2005, **109**, 3094-3096.
37. J. A. Coxon and P. G. Hajigeorgiou, *J. Molecular Spectroscopy*, 1991, **150**, 1-27.
38. M. D. Feit and J. A. Fleck, *The Journal of Chemical Physics*, 1983, **78**, 301-308.
39. N. Balakrishnan, C. Kalyanaraman and N. Sathyamurthy, *Phys. Rep.*, 1997, **280**, 79-144.
40. B. Friedrich, personal communication.

Conflicts to declare

There are no conflicts to declare.

Acknowledgements

This material is based upon work supported by the National Science Foundation under Grant No. 1464640 and Grant No. 1806334. K.H., J.M., and M.S. are grateful to Dr. Bretislav Friedrich, Fritz-Haber Institute, Berlin, Germany for useful discussions. N.B. is grateful to Keith Lawler for his assistance with computations of excited state polarizabilities of HI presented in the supplementary material.

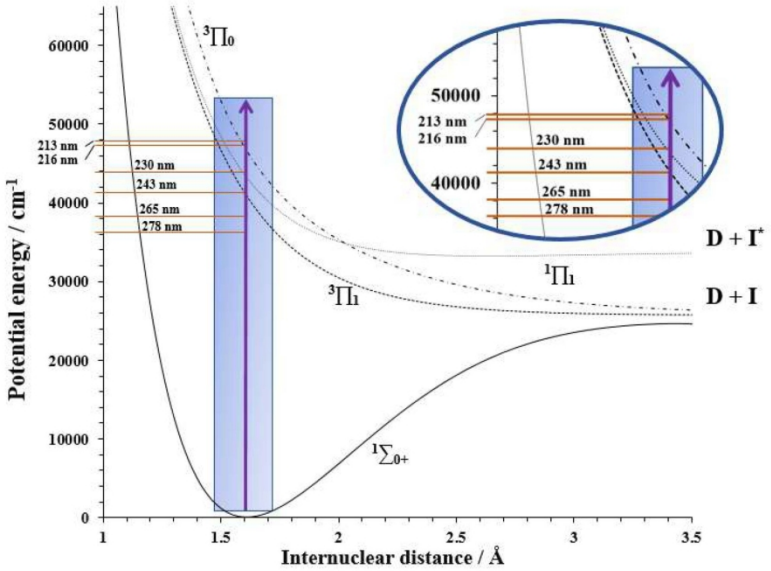

Fig. 1 Potential energy curves for the ground and low-lying excited electronic states of DI involved in one-photon dissociation. The parts of the potential that were sampled at each experimental excitation wavelength, within the Franck-Condon region, are illustrated schematically.

279x215mm (300 x 300 DPI)

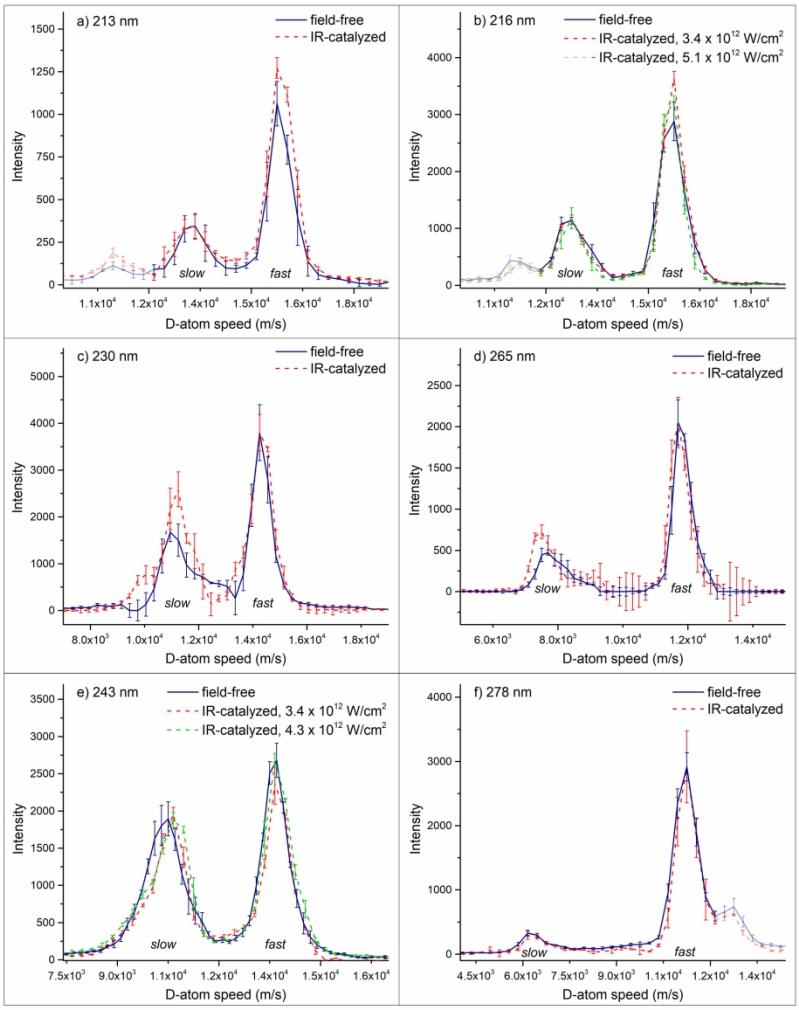

Fig. 2 D-atom speed distributions for the photodissociation of DI at a series of excitation wavelengths: a) 213 nm, b) 216 nm, c) 230 nm, d) 265 nm, e) 243 nm, and f) 278 nm. The blue lines represent data collected in the absence of a strong electric field (field-free), and the red dashed lines represent data collected at an IR peak intensity of 3.4×10^{12} W/cm^2 ($\mathcal{E}_0 = 5.1 \times 10^7$ V/cm, IR-catalyzed). The green dashed lines in b) and e) are for experiments performed at higher IR peak intensities of 4.3×10^{12} W/cm^2 and 5.1×10^{12} W/cm^2, respectively ($\mathcal{E}_0 = 5.8 \times 10^7$ V/cm, and 6.3×10^7 V/cm). Error bars denote one standard deviation over 3-5 experimental data sets. A third peak is observed in the case of Fig. 2a, 2b, and 2f, here marked in a lighter shade for clarity, which originates from photolysis by the complementary Doppler-free probe laser. The shoulders on the leading edges of the fast and slow channel peaks in Fig. 2c are also consistent with 243-nm dissociation by the probe laser.

203x271mm (300 x 300 DPI)

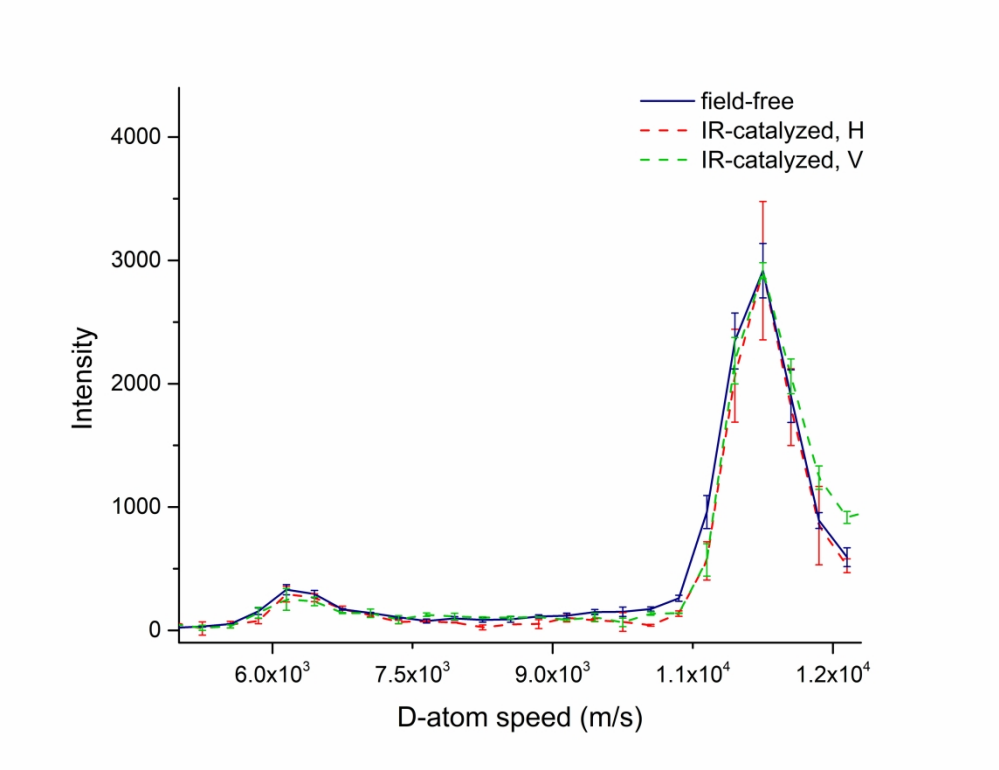

Fig. 3 D-atom speed distributions for the photodissociation of DI at 278 nm in the absence (blue line) and presence of vertically polarized (red dashed line) and horizontally polarized (green dashed line) IR field. Error bars denote one standard deviation over 3-5 experimental data sets.

279x215mm (300 x 300 DPI)

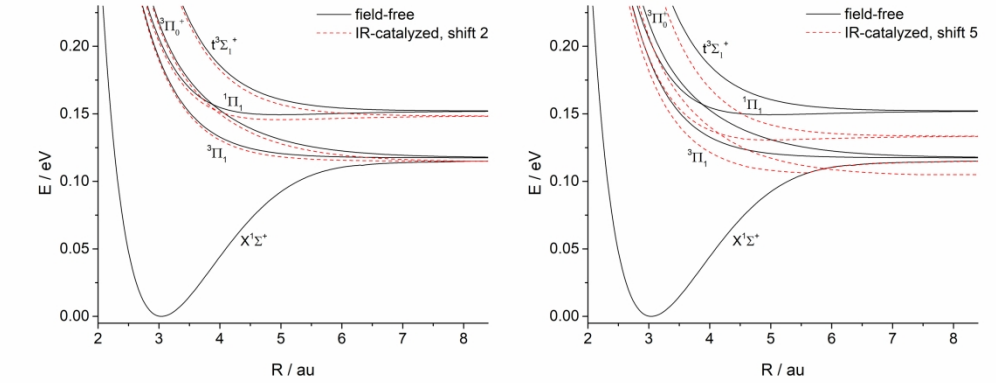

Fig. 4 Potential energy curves for the one-photon dissociation of DI under field-free (black, solid) and IR-catalyzed (red, dashed) conditions using the polarizabilities of a) shift 2 and b) shift 5. The electric field strength for these calculations was 5.1×10^7 V/cm.

279x215mm (300 x 300 DPI)

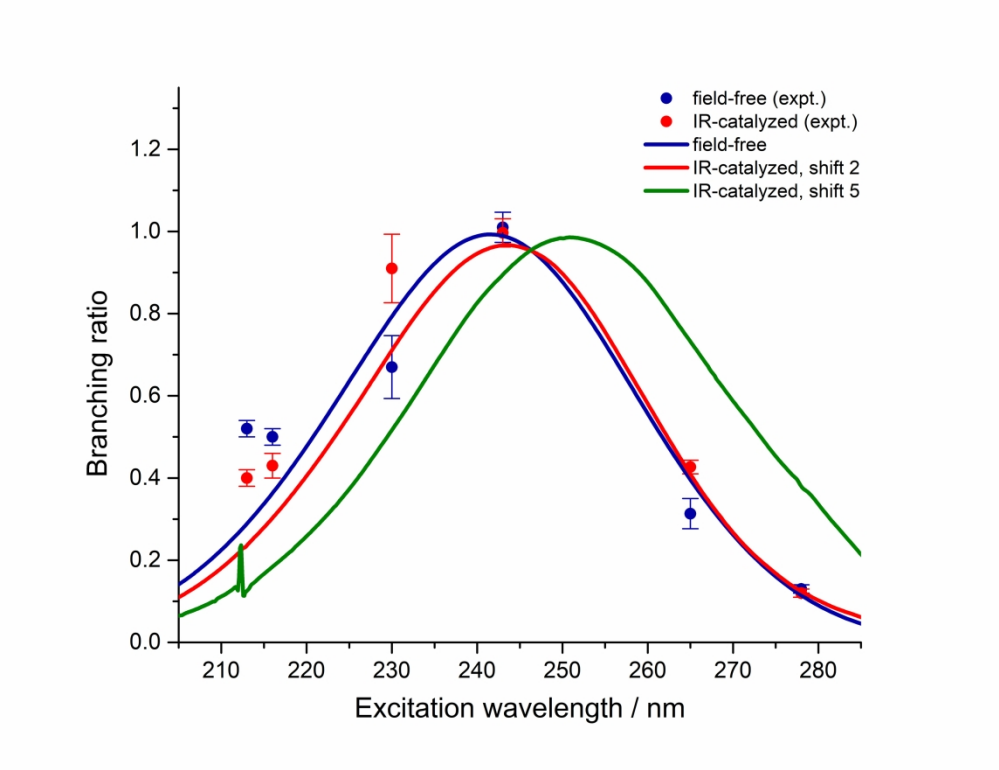

Fig. 5 Experimentally and theoretically determined branching ratios for the photolysis of DI, both in the presence (red and green) and absence (blue) of the strong IR field at 5.1×10^7 V/cm. Results of calculations for shifts 2 (red) and 5 (green) are displayed. Error bars denote one standard deviation over 3-5 experimental data sets.

279x215mm (300 x 300 DPI)

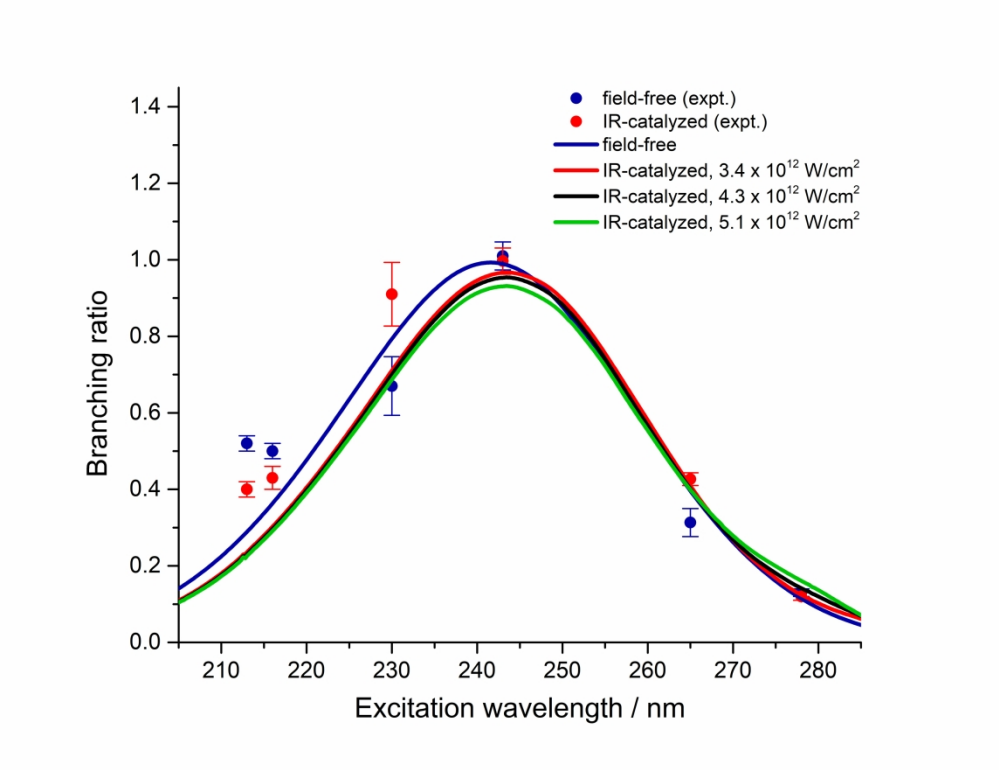

Fig. 6 Theoretically calculated branching ratio curves for the dissociation of DI under field-free conditions (black) and in the presence of a nonresonant IR field at 5.1×10^7 V/cm (red, 3.4×10^{12} W/cm^2), 5.8×10^7 V/cm (blue, 4.3×10^{12} W/cm^2), and 6.3×10^7 V/cm (green, 5.1×10^{12} W/cm^2). Error bars denote one standard deviation over 3-5 experimental data sets.

279x215mm (300 x 300 DPI)

The photodissociation of deuterium iodide is catalyzed by the electric field supplied by nonresonant IR photons.

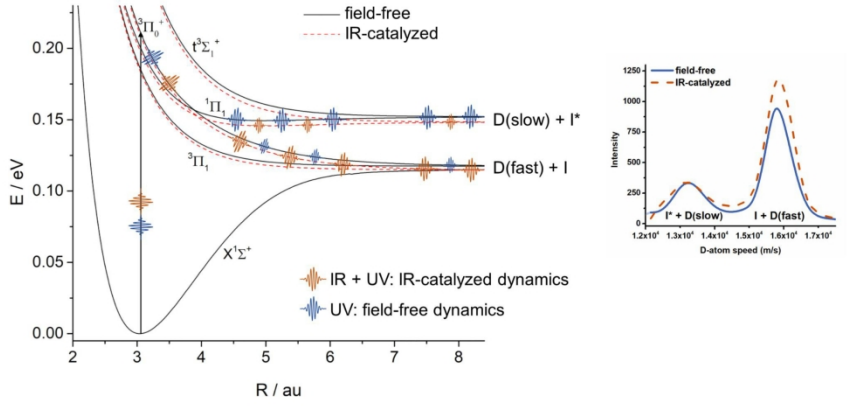

279x215mm (300 x 300 DPI)

Electronic Supplementary Information

Photon catalysis of deuterium iodide photodissociation

Kallie I. Hilsabeck [†a], Jana L. Meiser [†a], Mahima Sneha [†a], N. Balakrishnan[b], Richard N. Zare[a*]

[a] Department of Chemistry, Stanford University, Stanford, CA, 94305, USA
[b] Department of Chemistry and Biochemistry, University of Nevada, Las Vegas, Las Vegas, NV, 89154, USA

[†] These authors contributed equally to this research.

All correspondence should be addressed to rnz@stanford.edu.

Supplementary Information Table of Contents

Description of Background Subtraction Method

Laser powers were chosen to minimize background associated with nonresonant, multiphoton dissociation and ionization processes – for example, absorption of IR + UV photons to produce D^+ ions. It should be noted that no signal was observed from absorption of the IR laser alone, as the laser's focal intensity was insufficient to cause multiphoton excitation or ionization of the molecules ion the interaction volume. Any remaining background was subtracted using the two-shot method, schematically illustrated in Figure S1.

In the first shot, raw signal was collected, consisting of both true signal and background events. For Doppler-free experiments, in the first shot, all three lasers (UV_1, UV_2, and IR) were overlapped in time (Figure S1a). For pump-probe experiments, the IR pulse was overlapped with the pump pulse, and the probe pulse was delayed by 3 ns (Figure S1b). The delay was used to reduce the multiphoton ionization process caused by the overlap of the IR and probe lasers, which was found to eliminate a major source of background. The specific time delay was optimized to 3 ns to both minimize multiphoton processes while also maximizing the ionization yield. This is important in our experiments because the D atoms are formed at a very high lab-frame speed and could otherwise escape the focal volume before ionization.

In the second shot, background signal was collected: the IR pulse was overlapped with only one of the UV lasers in time, UV_1. The remaining UV laser, UV_2, was offset by 50 ns so that no true signal from the pump-probe is generated in this shot. By subtracting the background signal from the raw signal, we accounted for nonresonant, multiphoton processes arising from overlap of the IR laser with UV_1. An illustrative representation of the speed distributions measured from the raw signal, background signal, and final signal are presented in Figure S1c. The advantage of the two-shot method is that it allows us to collect the background in the same scan as that of signal, thereby eliminating any discrepancies caused by laser power fluctuations between different sets of experiments.

For this two-shot method, the UV laser that was observed to produce the most background signal with the IR laser was assigned as UV_1. For most experiments, the laser power of UV_2 could be maintained at a power that contributed negligibly to nonresonant processes. However, when background from UV_2 + IR was observed, an additional background scan was performed to account for it. The background scan was collected under the same conditions as the signal scan, but with the UV_1 laser switched off. The speed distributions presented in this work represent the final signal: raw signal – background signal 1 (UV_1 + IR) – background signal 2 (UV_2 + IR).

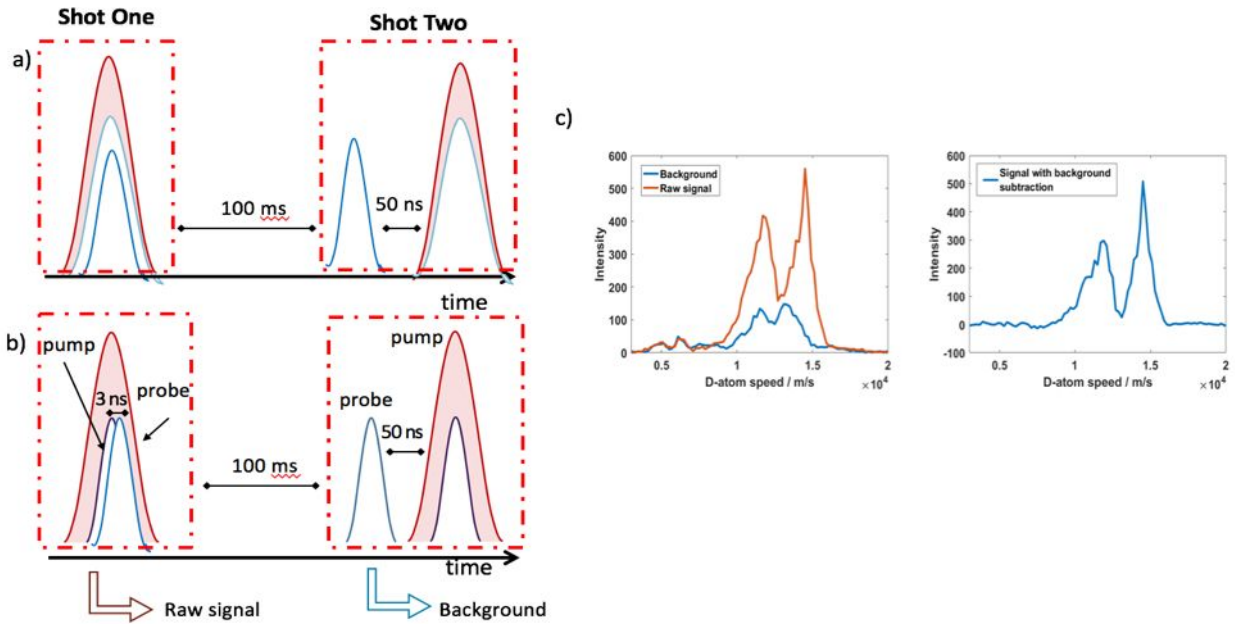

Fig. S1 Schematic diagram of the two-shot background subtraction method described in the text for the a) Doppler-free and b) pump-probe cases. The red curve represents the IR pulse, and the blue and purple curves represent the two UV laser pulses. c) Representative speed distributions for raw signal (left, orange), background signal (left, blue), and final signal = raw signal – background signal 1 (right, blue).

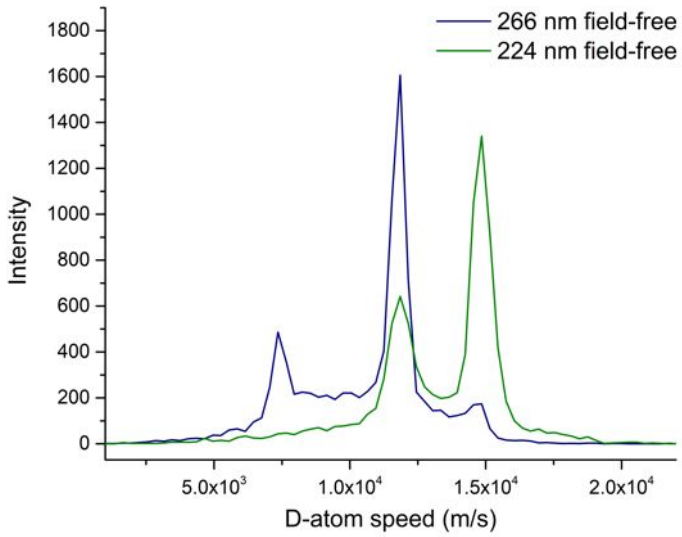

Fig. S2 D-atom speed distributions collected using the Doppler-free technique at excitation wavelengths of 266 nm (blue line) and 224 nm (green line) under field-free conditions. The slow channel produced at 224 nm clearly overlaps with the fast channel of 266 nm at our resolution of about 250 m/s, making it impossible to separate the two contributions to the total photodissociation. The speeds produced by 266-nm dissociation are very close to the speeds produced at 265 nm, and are used as justification for choosing the pump-probe technique.

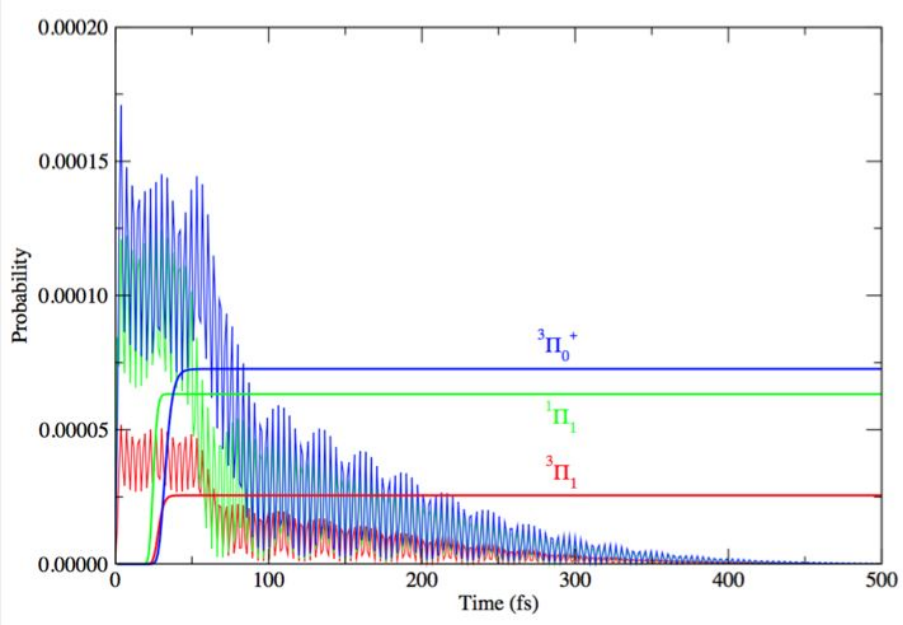

Fig. S3 Probability of excitation and dissociation on the three excited electronic states of DI, as a function of time. Both time-dependence of the probabilities and the time-integrated probabilities are shown.

Supporting Calculations for Polarizabilities of the Excited States of HI

Results of preliminary calculations of polarizabilities of HI were performed using equation of motion coupled cluster singles and doubles (EOM-CCSD) with Q-Chem[1]. These values are provided in Table S1. The computed values for the ground state are in close agreement with those reported by Maroulis.[2] The basis set used is the quadruple-ζ with extra polarization and diffuse functions (def2-QZVPPD) of Weigend and Ahlrichs.[3] The 28 electron def2 effective core potential that accounts for scalar relativistic effects was used for the iodine atom. The isotropic polarizability is calculated as $\frac{1}{3}(\alpha_{xx} + \alpha_{yy} + \alpha_{zz})$ while the anisotropic polarizability is evaluated as $\sqrt{\frac{1}{2}\left((\alpha_{xx} - \alpha_{yy})^2 + (\alpha_{yy} - \alpha_{zz})^2 + (\alpha_{zz} - \alpha_{xx})^2\right)}$. The scaled values of the polarizabilities adopted in the wave packet simulations, in particular, those corresponding to shift2, are generally consistent with the values for $^3\Pi$ and $^1\Pi$ states given in Table S1. More detailed calculations including spin-orbit coupling are beyond the scope of this work.

Table S1. Dipole moment and polarizabilities of the ground state and excited $^3\Pi$ and $^1\Pi$ states of HI corresponding to a bond distance of 3.04 bohr.

State	Excitation Energy (eV)	Excitation Energy (nm)	Dipole Moment (au)	Isotropic Polarizability (au)	Anisotropic Polarizability (au)
$^1\Sigma_{0+}$	0.00	0.00	0.182194	35.017	2.791
$^3\Pi$	5.1981	238.52	0.277526	54.034	53.911
$^1\Pi$	5.7064	217.27	0.232328	66.225	77.184

(1) Shao, Y.; Gan, Z.; Epifanovsky, E.; Gilbert, A. T. B.; Wormit, M.; Kussmann, J.; Lange, A. W.; Behn, A.; Deng, J.; Feng, X.; et al. Advances in Molecular Quantum Chemistry Contained in the Q-Chem 4 Program Package. *Mol. Phys.* **2015**, *113* (2), 184–215.

(2) Maroulis, G., Is the dipole polarizability of hydrogen iodide accurately known? *Chem. Phys. Lett*. 2**000**, 318, 181.

(3) Weigend, F.; Ahlrichs, R. Balanced Basis Sets of Split Valence, Triple Zeta Valence and Quadruple Zeta Valence Quality for H to Rn: Design and Assessment of Accuracy. *Phys. Chem. Chem. Phys.* **2005**, *7* (18), 3297.

Table S2. D-atom slow and fast channel peak speeds measured at different excitation wavelengths, using a (2+1) REMPI detection scheme centered approximately at 243 nm.

Pump wavelength (nm)	Probe wavelength (nm)	v_fast (m/s)	v_slow (m/s)
213*	213, 283	15800	13300
216*	216, 278	15800	12800
224*	266	14800	11900
230	243	14300	11100
243*	243	13700	10500
265	243	11700	7600
266*	224	11900	7700
278*	278, 216	11300	6200

* For the measurements using the Doppler-free probing technique, the UV lasers are set at wavelengths such that together they are resonant to the 2s←1s two photon excitation of the D atom.

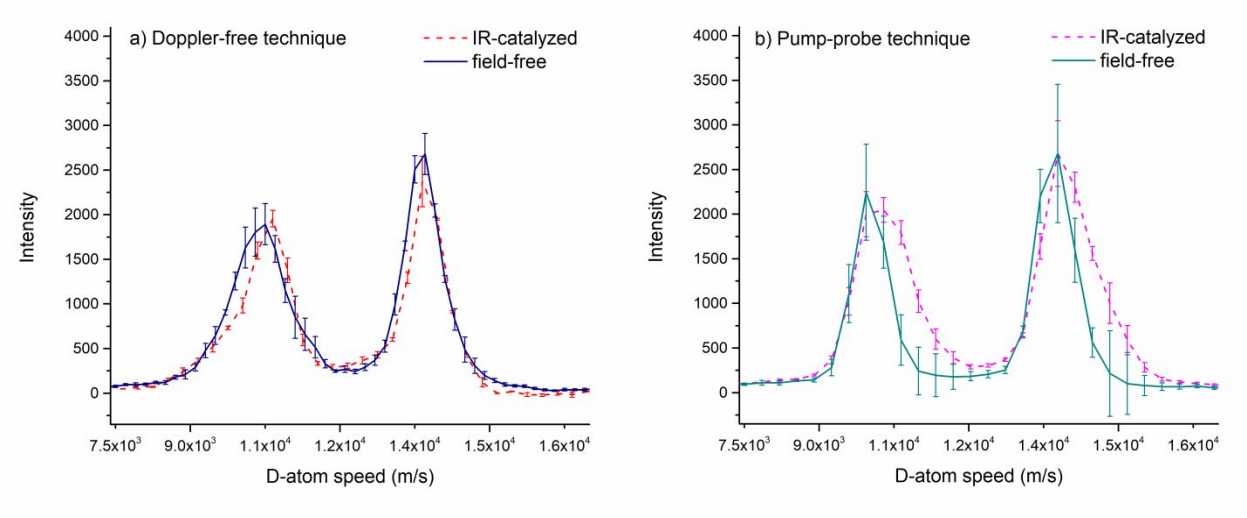

Fig. S4 D-atom speed distributions collected at an excitation wavelength of 243 nm using a) the Doppler-free technique (blue solid line – field-free, red dashed line – IR-catalyzed) and b) the pump-probe technique (turquoise solid line – field-free, pink dashed line – IR-catalyzed). The relative branching ratio change with the application of the electric field, i.e. no significant change to one standard deviation, is the same for both detection techniques, despite the apparent widening of the peaks in the presence of the IR field in b). Although the measured effect of the IR field was the same for both techniques, the Doppler-free data were chosen for presentation in the manuscript for two reasons: the absolute branching ratio under field-free conditions more closely approximated previous experimental and theoretical results, and the cleaner experimental setup gave well-defined Gaussian peaks in the speed distribution.

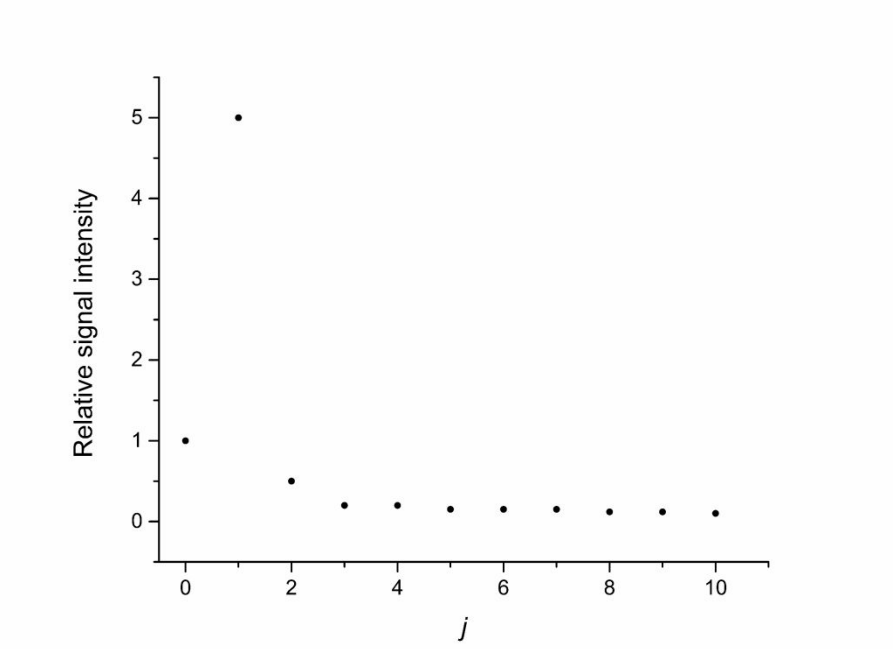

Fig. S5 Estimate of DI rotational distribution of molecules in lower *j* levels in the molecular beam. There is detectable population up to *j* = 10, measured by DI (2+1) REMPI.